Available online at www.sciencedirect.com
SCIENCE DIRECT
Geochimica et Cosmochimica Acta 70 (2006) 3239–3260
Geochimica
www.elsevier.com/locate/gca

Trace element fractionation and transport in boreal rivers and soil porewaters of permafrost-dominated basaltic terrain in Central Siberia

O.S. Pokrovsky *, J. Schott, B. Dupré

Laboratoire des Mécanismes et Transfert en Geologie (LMTG), UMR 5563, CNRS-UPS-IRD—Observatoire Midi-Pyrenées, 14 Avenue Edouard Belin, 31400 Toulouse, France

Received 15 November 2005; accepted in revised form 6 April 2006

Abstract

The chemical status of ~40 major and trace elements (TE) and organic carbon (OC) in pristine boreal rivers draining the basaltic plateau of Central Siberia (Putorana) and interstitial solutions of permafrost soils was investigated. Water samples were filtered in the field through progressively decreasing pore size (5 μm → 0.22 μm → 0.025 μm → 10 kDa → 1 kDa) using cascade frontal filtration technique. Most rivers and soil porewaters exhibit 2–5 times higher than the world average concentration of dissolved (i.e., <0.22 μm) iron (0.03–0.4 mg/L), aluminum (0.03–0.4 mg/L), OC (10–20 mg/L) and various trace elements that are usually considered as immobile in weathering processes (Ti, Zr, Ga, Y, REEs). Ultrafiltration revealed strong relationships between concentration of TE and that of colloidal Fe and Al. According to their partition during filtration and association with colloids, two groups of elements can be distinguished: (i) those weakly dependent on ultrafiltration and that are likely to be present as truly dissolved inorganic species (Li, Na, K, Si, Mn, Mo, Rb, Cs, As, Sb) or, partially (20–30%) associated with small size Fe- and Al-colloids (Ca, Mg, Sr, Ba) and to small (<1–10 kDa) organic complexes (Co, Ni, Cu, Zn), and (ii) elements strongly associated with colloidal iron and aluminum in all ultrafiltrates largely present in 1–100 kDa fraction (Ga, Y, REEs, Pb, V, Cr, Ti, Ge, Zr, Th, U). TE concentrations and partition coefficients did not show any detectable variations between different colloidal fractions for soil porewaters, suprapermafrost flow and surface streams. TE concentration measurements in river suspended particles demonstrated significant contribution (i.e., ⩾30%) of conventionally dissolved (<0.22 μm) forms for usually "immobile" elements such as divalent transition metals, Cd, Pb, V, Sn, Y, REEs, Zr, Hf, Th. The Al-normalized accumulation coefficients of TE in vegetation litter compared to basalts achieve 10–100 for B, Mn, Zn, As, Sr, Sn, Sb, and the larch litter degradation is able to provide the major contribution to the annual dissolved flux of most trace elements. It is hypothesized that the decomposition of plant litter in the topsoil horizon leads to Fe(III)-, Al-organic colloids formation and serves as an important source of elements in downward percolating fluids.

1. Introduction

The development, over the past twenty years, of high-resolution analytical instrumentation has generated important progress in characterizing the behavior of trace elements (TE) in various surficial aquatic environments (see for review Gaillardet et al., 2003). In many studies the distinction between dissolved and particulate loads was based on filtration using 0.45 or 0.22 μm poresize membranes. However, it is well known that in natural waters, many trace elements are present in colloidal (i.e., between 1 nm and 1 μm) rather than true dissolved forms (Buffle et al., 1992). As a result, ultrafiltration techniques with membranes of different pore sizes are increasingly used to characterize the proportion of dissolved and colloidal forms in surficial aquatic environments such as seawater, rivers and lakes (Hoffman et al., 1981, 2000; Benoit, 1995; Guo and Santschi, 1996; Lead et al., 1997; Dupré et al., 1999; Eyrolle and Benaim, 1999; Ross and Sherrell, 1999; Olivié-Lauquet et al., 1999, 2000; Ingri et al., 2000, 2004; Sigg et al., 2000). Subsequently, several studies have determined the thermodynamic parameters of metal complexation with colloidal matter (Tipping, 1994; Benedetti

* Corresponding author. Fax: +33 5 61 33 25 60.
E-mail address: oleg@lmtg.obs-mip.fr (O.S. Pokrovsky).

0016-7037/$ - see front matter © 2006 Published by Elsevier Inc.
doi:10.1016/j.gca.2006.04.008

et al., 1995; Johannesson et al., 2004; Sonke and Salters, 2006). This paper represents part of a concerted effort conducted in our laboratory to characterize the colloidal transport of TE in various "pristine" aquatic environments. Previous works addressed the speciation and transport of TE in tropical (Viers et al., 1997; Braun et al., 1998; Dupré et al., 1999) and boreal (Pokrovsky and Schott, 2002) rivers, and in temperate peat soil porewaters (Pokrovsky et al., 2005a). In the current study, boreal rivers and soil porewaters from permafrost regions of basaltic lithology were investigated. Among crystalline rocks, basalts are particularly sensitive to chemical erosion and exert a significant impact on the geological carbon cycle and hence on climate (Dupré et al., 2003). Whereas numerous mineralogical and geochemical studies have addressed major element behavior and fluxes during basalt weathering (Pokrovsky et al., 2005b and references therein), transport of trace elements and organic carbon involved in this process has received much less attention.

In contrast to the important efforts centered on TE behavior in temperate and tropical environments, boreal permafrost-dominated areas remained, up to present time, essentially ignored by aquatic geochemists. Such remote regions represent one of the most important reservoirs of terrestrial organic carbon in the form of peat and organic-rich soils located in the glaciated environment (Botch et al., 1995; Peng et al., 1998). As a result, migration of many TE in such organic-rich waters is likely to occur in the form of organo-mineral colloids as demonstrated by studies conducted in the mouth's of large Siberian rivers (e.g., Martin et al., 1993; Dai and Martin, 1995). Geochemistry of TE during permafrost thawing and organic carbon mobilization induced by global warming are the main issues affecting such boreal regions. Continuing increase of river runoff in the Russian Arctic drainage basin over the past several decades (Serreze et al., 2002) and release of carbon and metals trapped in the permafrost ice (i.e., Guo et al., 2004) is likely to modify the fluxes of chemical elements to the ocean and their forms in river and soil porewaters. Under conditions of global warming, the short-term DOC production in forest floor environments will increase (Prokushkin et al., 2005) thus increasing the proportion of trace metals complexed by organic ligands. Several previous studies of Arctic watersheds underlain by permafrost addressed the behavior of organic carbon and major mineral nutrients (Lock and Ford, 1986; Peterson et al., 1986, 1992; Lock et al., 1989; Everett et al., 1996; Oswood et al., 1996). Important conclusions drawn in these earlier studies include the recognition that the stream chemistry in permafrost-dominated watersheds is tightly coupled to the chemistry of organic horizons in the upper soil due to limited contact between water and bottom soil horizons (MacLean et al., 1999).

Except for a few studies of soil and river solute migration in Alaska (Brown et al., 1962; Ugolini et al., 1987; Shiller, 2003; Rember and Trefry, 2004) and trace elements measurements in the Russian Arctic (Dai and Martin, 1995; Guieu et al., 1996; Moran and Woods, 1997; Zhulidov et al., 1997), studies addressing colloidal vs. dissolved forms and transport of TE in organic-rich waters from pristine permafrost landscapes are scarce. In this paper, we characterize the size of colloids and quantify the fluxes of TE through a thorough study of large and small river watersheds, ground and soil porewater solutions that issue from remote permafrost-dominated territory underlain by basaltic rocks. We address the following questions:

(i) what is the proportion of colloidal TE in surficial fluids and in which part of the soil profile are these colloids formed?
(ii) can we distinguish between adsorbed and incorporated TE and organically complexed TE in these colloids?
(iii) what is the source of TE in rivers (rock, soil minerals, plant litter, permafrost ice)?
(iv) how does the presence of permafrost affect the vertical and lateral migration of TE in boreal regions?

2. Sampling and analyses

The sampling area is located in the northern part of Central Siberia, within the drainage basin of the Nizhniya Tunguska River (eastern tributary of the Yenissey River) on the basaltic plateau of Putorana (64–70°N; 88–102°E). Detailed geological, climatic and geographic descriptions of the region and sample characteristics are given in Pokrovsky et al. (2005b). Altogether, 10 large rivers (for each, the drainage basin at the sampling point is larger than 10,000 km^2), 50 medium size rivers (1000–10,000 km^2) and 30 small creeks (<1000 km^2), 20 soil porewaters and 10 groundwaters (suprapermafrost flow samples) were collected during July–August 2001 (Fig. 1). The majority of the samples (75%) belong to the watershed of the river Kochechumo (right tributary of the river Nizhniya Tunguska, Yenissey basin). The studied region, because of its limited access and absence of any agricultural and industrial activity, can be considered, for most trace elements, as a pristine environment with background abundances in rivers, although the atmospheric deposition of heavy metals (e.g., Hg, Pb, Zn) cannot be totally ruled out.

River samples (shown by solid circles in Fig. 1) were collected from the beach or via a rubber boat near the middle of the stream flow in pre-cleaned 1-L high-density polyethylene (HDPE) containers connected to a non-metallic stick. Groundwater samples corresponding to the suprapermafrost flow (triangles in Fig. 1) were collected from the border of river valleys or canyons, at depths of 30–100 cm over the permafrost table. Soil porewaters (squares in Fig. 1) were extracted from humid soil horizons in the field using a Ti pressure device (Pokrovsky et al., 2005b). Depending on the saturation state of soil samples, 10–50 mL of solutions were collected.Typically, 1 dm^3 of solid soil sample yielded 30–70 mL of interstitial pore water. After each

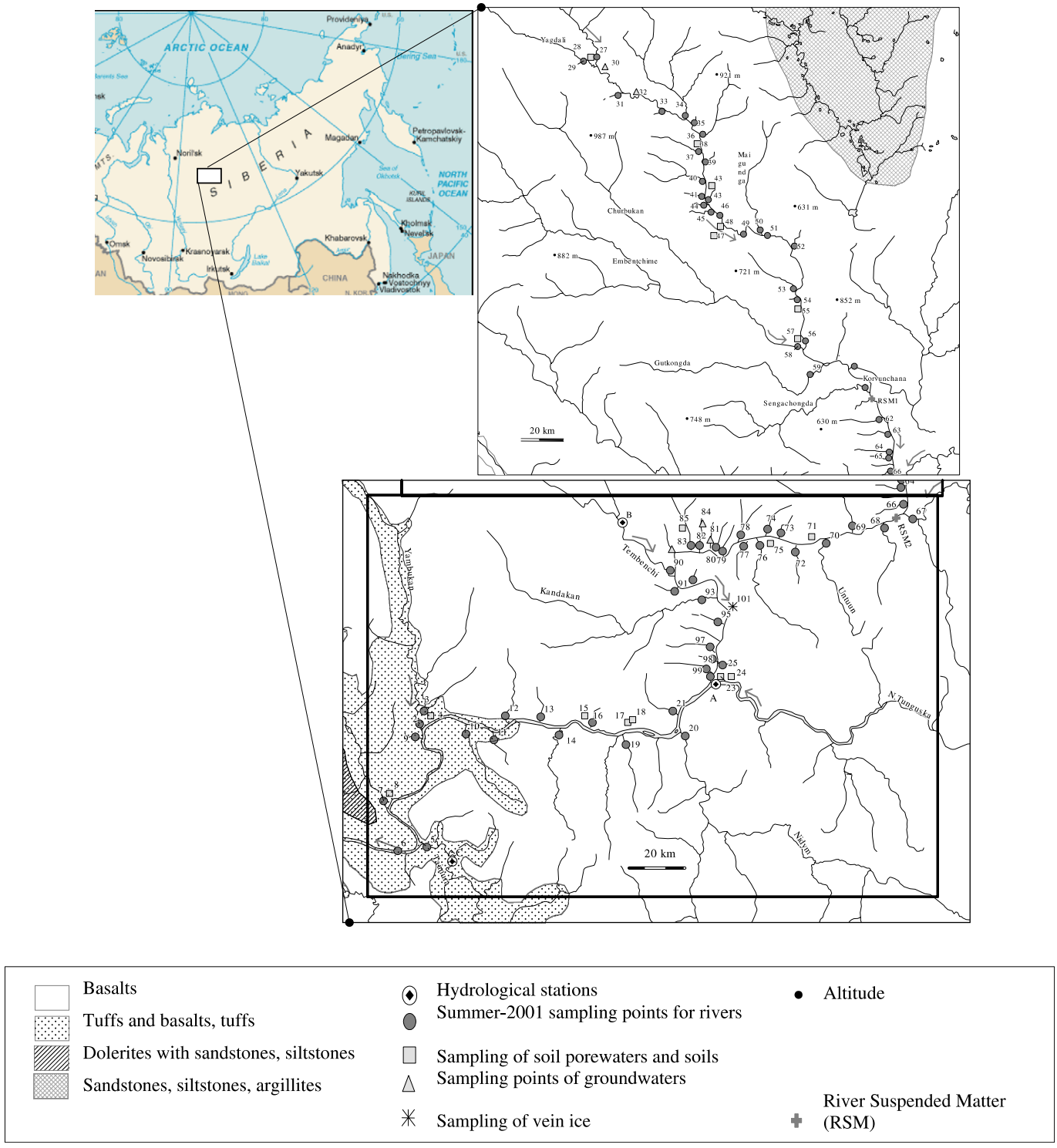

Fig. 1. Map of the area showing rivers, sampling points and geology.

extraction, the vessel and its compartments were thoroughly washed by riverwater followed by 100–200 mL of distilled water. Before and after fieldwork, blank samples were run by filling the pressure system with MilliQ (18 $M\Omega cm^{-1}$) water at neutral pH and letting it react for 24 h. No detectable contamination of major and trace elements and DOC was observed. Plastic gloves were always used during all sample collections.

The value of pH was measured using a combined Schott-Geräte electrode calibrated against NIST buffer solutions (pH = 4.00, 6.86 and 9.18 at 25 °C) with an accuracy of ±0.02 pH units. The collected waters were immediately filtered through 0.22 μm acetate cellulose membranes (47-mm diameter) using a precleaned Sartorius polycarbonate filter holder. Only filtered (<0.22 μm) waters were used in the ultrafiltration steps in series

0.22 μm → 0.025 μm → 10 kDa → 1 kDa according to the cascade ultrafiltration procedure. Filtrations were carried out using a MITYVAC® manual pump providing 1.2–1.5 atm pressure. The first 200–400 mL of the filter-passed permeate (referred to as filtrate) were systematically rejected. Ultrafiltrations through 0.025 μm, 10 kDa and 1 kDa membranes (Amicone, regenerated cellulose, 200 μm thickness and 45 mm in diameter) were performed using a Sartorius filter holder. A typical ultrafiltration step lasted from 6 h (for 0.025 μm and 10 kDa pore size) to 12 h (for 1 kDa pore size) such that 300–500 mL of <0.22 μm initial filtrate produced ~50 mL of <1 kDa ultrafiltrate. Before each filtration, the system was cleaned by flushing MilliQ water, then ~0.1 M ultrapure HNO_3, and finally, MilliQ water. During filtration, the first 30–50 mL of filtrate was discarded. Each filter was washed in MilliQ water before each collection and was used only once. For each filtration, the filter was replaced by a new one when a substantial decrease in the flow rate occurred indicating membrane clogging (i.e., Morrison and Benoit, 2001). This greatly decreased the probability of cross-contamination during sample filtration, improved the DOC blank, and allowed high recovery of colloidal particles. For several frontal ultrafiltrations, the retentate was collected for mass balance analyses. In all cases, better than 95% recovery for major elements, organic carbon, Al, Fe and 90% recovery for selected trace elements (Ti, Sr, Y, Ba, Zr) was achieved indicating that the adsorption of colloids and associated TE inside the thin membrane was negligible. We also calculated the mass balance between the initial (i.e., <0.22 μm or <5 μm) solution and various filter-passing permeates (<1 kDa, <10 kDa, <0.025 μm) for organic carbon, major elements and some trace elements (Fe, Al, Ti, Mn, Cu, Zn, Y, Sr, Ba, La, Ce, Th). The total recovery was better than 90% except in several samples for Cu, Zn and Pb when a clear contamination was observed as indicated in Table 1. Further discussions and precautions taken against possible artifacts of filtration are given in Pokrovsky and Schott (2002) and Pokrovsky et al. (2005a). Filtered and ultrafiltered solutions for major cation and trace element analyses were acidified (pH 2) with ultrapure double-distilled HNO_3 and stored in HDPE bottles previously washed with ultrapure 0.1 M HCl and rinsed with MilliQ water. The preparation of bottles for sample storage was performed in a clean room. The samples for DOC analyses were collected in pyrolyzed Pyrex glass tubes in which $HgCl_2$ (10 mg/L) was added to prevent bacterial development. The MilliQ field blanks were collected and processed in order to evaluate potential sample contamination introduced by our sampling and handling procedure. Organic carbon blanks of filtrate and ultrafiltrates never exceeded 0.1 mg/L, which is low for the organic-rich rivers sampled in this study (typically, 5–20 mg/L DOC). For all major and most trace elements, concentrations in blanks were below analytical detection limits (⩽0.1–1 ng/L for Cd, Ba, Y, Zr, Nb, REE, Hf, Pb, Th, U; 1 ng/L for Ga, Ge, Rb, Sr, Sn, Sb; ~10 ng/L for Ti, V, Cr, Mn, Fe, Co, Ni, Cu, Zn, As). In several cases, however, clear contamination by Zn, Cu, Ni and Pb was detected in 10 kDa and 1 kDa ultrafiltrates as their concentration in 1 kDa and 10 kDa UF were >20% higher than those in <0.22 μm fraction. These samples were not considered in the analysis of results.

Aqueous silica concentration was determined colorimetrically (molybdate blue method) with an uncertainty of 2% using a Technicon automated analyzer. Alkalinity was measured by potentiometric titration with HCl to pH 4.2 using the Gran method, with a detection limit of 10^{-5} M and an uncertainty of 2%. DOC was analyzed using a Carbon Total Analyzer (Shimadzu TOC 5000) with an uncertainty better than 3%. Major anion concentrations (Cl, SO_4, F, NO_3) were measured by ion chromatography (HPLC, Dionex 2000i) with an uncertainty of 2%. Calcium, magnesium, sodium and potassium concentrations were determined by atomic absorption spectroscopy (AAS; Perkin-Elmer 5100PC analyzer) with an uncertainty of 1–2%. High concentrations of dissolved iron (i.e., >0.5 mg/L) were measured by flame AAS, whereas the lower concentrations were measured by ICP-MS (Elan 6000, Perkin-Elmer) and by flameless AAS (Perkin-Elmer 5100PC). Trace elements (TE) were measured without preconcentration by ICP-MS. For several ultrafiltrates having very low TE concentration, an automated desolvator was used, which decreased the detection limit by a factor of 5. Indium and rhenium were used as internal standards and corrections for oxide and hydroxide ions were made for REEs and other trace elements (Aries et al., 2000). The international geostandard SLRS-4 (Riverine Water Reference Material for Trace Metals certified by the National Research Council of Canada) was used to check the validity and reproducibility of the analyses (Yeghicheyan et al., 2001). Good agreement between our replicated measurements of SLRS-4 and the certified values was obtained (relative difference <10%) except for B and P (30%). For many samples of surficial fluids and ultrafiltrates having very low concentrations of TE, on the order of 0.001 μg/L comparable with detection limits such as Ag, Cd, Hf, Ge, Cs, Ga, Se, Sn, Nb, Ta, W, Tl, Bi reliable measurements were not possible.

Finely crushed soil and river suspended matter samples collected via frontal filtration through 0.22 μm filter were dissolved by acid (ultrapure HF, HNO_3) in Teflon Savillex vials; BE-N basalt rock standard was dissolved under the same conditions. Vegetation samples (moss, lichens and larch litter) were rinsed by MilliQ water in the field, dried at 60 °C in the laboratory and subjected to $H_2O_2 + HNO_3$ digestion at room temperature followed by $HNO_3 + HF$ on a hot plate to provide entire dissolution of all solid phases. Different mineral soil horizons and organic-rich topsoils were dried at 90 °C and treated in the same way, but without MilliQ rinsing. International vegetation and sediment standards (SRM 1515 apple leaves and LKSD-1 lake sediment powder, respectively) were prepared at the same time as samples. All treatment of solid samples for ICP-MS analysis was performed in a clean room. Good agreement between our replicated measurements of

Table 1
Results of frontal cascade filtration and ultrafiltration

Sample	OC	Mg	Ca	Si	Na	SO_4	Li	Al
31–1 kDa	5,500	1,450	3,270	5,370	843	128	0.28	12
31–0.025 μm	9,000	1,812	4,510	6,510	939	ND	0.28	52
31–0.22 μm	10,800	1,800	4,310	6,590	953	187	0.28	53
31–5 μm	10,900	1,847	4,610	6,690	903	ND	0.29	285
47–1 kDa	12,400	783	2,100	8,066	978	292	0.09	156
47–0.025 μm	13,000	788.7	2,170	8,050	981	ND	0.10	804
47–0.22 μm	5,000	578	1,360	8100	861	274	0.10	819
57–1 kDa	25,100	2,788	3,190	6,040	899	ND	0.17	134
57–10 kDa	25,800	3,250	3,920	6,110	954	ND	0.17	384
57–0.025 μm	28,200	3,450	4,240	6,050	940	ND	0.19	779
57–0.22 μm	27,800	3,460	4,320	6,070	963	ND	0.19	819
57–2.5 μm	27,300	3,510	4,390	6,040	967	ND	0.17	802
57–5 μm	27,700	3,540	4,490	6,110	968	ND	0.15	860
60–1 kDa	12,700	1,810	4,180	6,280	2,286	588	0.10	7
60–10 kDa	13,300	1,790	4,240	6,250	2,225	527	0.10	23
60–0.025 μm	12,400	1,790	4,160	6,380	2260	571	0.11	43
60–0.22 μm	10,100	1,600	3,520	5,750	2,160	570	0.10	46
67–1 kDa	16,000	1,993	7,230	6,860	2,340	257	0.10	25
67–10 kDa	14,100	1,984	7,250	6,850	2,340	280	0.09	35
67–0.025 μm	13,500	1,980	7,120	6,950	2,320	285	0.10	47
67–0.22 μm	11,200	1,705	6,000	6,700	2,170	247	0.13	55
87–1 kDa	18,400	1,870	4,300	8,110	2,970	124	<d.l.	20
87–10 kDa	18,500	2,000	4,450	7,930	3,080	217	<d.l.	33
87–0.025 μm	18,300	2,072	4,910	8,330	3,110	251	<d.l.	49
87–0.22 μm	18,000	2,080	5,030	7,900	3,180	328	<d.l.	64
91–1 kDa	22,000	2,420	9,780	8,840	3,300	408	<d.l.	11
91–10 kDa	18,800	2,380	7,520	8,700	3,300	ND	<d.l.	33
91–0.025 μm	17,400	2,290	7,400	8,300	3,250	ND	<d.l.	46
91–0.22 μm	15,500	2,004	7,260	8,560	3,112	ND	<d.l.	64
93–1 kDa	10,600	1,800	6,460	8,420	3,610	743	<d.l.	12
93–10 kDa	14,100	1,949	6,930	9,700	3,770	667	<d.l.	29
93–0.025 μm	14,500	2,000	7,230	9,050	3,750	742	<d.l.	32
93–0.22 μm	14,400	1,980	7,170	9,430	4,270	774	<d.l.	43
96–10 kDa	13,900	2,216	6,120	6,670	2,920	ND	0.08	23
96–100 kDa	13,500	2,150	6,080	6,250	3,090	480	0.08	24
96–0.22 μm	12,500	2,229	6,180	6,150	2,900	ND	0.08	25
96–2.5 μm	12,000	2,193	5,860	6,220	2,840	487	0.07	30
20–1 kDa	10,200	3,725	38,300	6,170	18,200	4,650	0.95	12
20–0.025 μm	10,200	3,774	38,200	6,100	18,500	ND	1.01	14
20–0.22 μm	10,300	3,689	37,900	6,030	17,400	4,220	0.88	14
10–1 kDa	17,600	1,661	8,630	7,110	7,030	1,070	0.42	61
10–0.025 μm	19,100	1,735	9,230	7,120	7,480	1,060	0.53	100
10–0.22 μm	19,200	1,697	9,250	7,330	7,800	1,040	0.46	134

Element	Ti	V	Cr	Mn	Fe	Co	Ni	Cu
31–1 kDa	0.14	0.54	0.22	10.2	23	0.058	0.65	1.60
31–0.025 μm	0.77	0.58	0.57	11.8	107	0.094	1.43	4.71
31–0.22 μm	0.91	0.60	0.62	14.7	188	0.118	1.54	5.08
31–5 μm	1.82	0.82	0.66	15.6	359	0.118	1.63	4.52
47–1 kDa	0.24	0.26	0.03	1.7	17	0.079	0.11	1.18
47–0.025 μm	1.96	0.40	0.26	1.8	115	0.153	0.19	3.04
47–0.22 μm	2.19	0.40	0.33	1.7	125	0.164	0.28	2.99
57–1 kDa	0.33	0.69	0.51	31.1	40	0.463	1.90	1.64
57–10 kDa	1.34	0.97	0.81	38.2	193	0.736	2.89	2.40
57–0.025 μm	4.64	1.65	1.00	41.8	1015	0.874	3.18	2.53
57–0.22 μm	5.34	1.80	1.03	43.1	1122	0.907	3.43	2.63
57–2.5 μm	5.34	1.85	1.03	45.5	1155	0.998	3.48	2.71
57–5 μm	5.59	2.39	1.11	64.7	1405	1.20	3.47	2.97

(*continued on next page*)

Table 1 (*continued*)

Element	Ti	V	Cr	Mn	Fe	Co	Ni	Cu
60–1 kDa	0.14	0.51	0.17	ND	19	0.043	0.63	1.44
60–10 kDa	0.47	0.58	0.34	ND	44	<d.l.	1.02	2.56
60–0.025 μm	0.92	0.59	0.40	ND	72	<d.l.	1.03	2.58
60–0.22 μm	1.53	0.65	0.39	1.1	83	0.050	1.09	2.67
67–1 kDa	0.70	0.79	0.24	ND	42	0.057	0.74	1.66
67–10 kDa	0.78	0.86	0.46	ND	61	0.062	1.28	3.06
67–0.025 μm	1.15	0.89	0.51	1.2	86	0.062	1.51	3.48
67–0.22 μm	1.71	0.94	0.55	1.5	108	0.062	1.56	3.44
87–1 kDa	0.72	1.69	0.48	3.9	37	0.088	1.15	4.03
87–10 kDa	1.32	1.83	0.55	4.1	64	0.096	1.38	4.84
87–0.025 μm	2.22	1.92	0.63	4.6	111	0.111	1.51	5.76
87–0.22 μm	2.72	1.94	0.70	8.1	125	0.136	1.57	5.73
91–1 kDa	0.40	1.59	0.46	5.3	22	0.084	0.89	2.52
91–10 kDa	1.22	1.73	0.69	6.6	56	0.123	1.41	4.34
91–0.025 μm	2.00	1.81	0.73	7.0	90	0.136	1.50	5.07
91–0.22 μm	2.91	1.79	0.72	6.1	110	0.143	1.54	5.05
93–1 kDa	0.63	1.50	ND	ND	31	ND	1.01	3.11
93–10 kDa	1.17	1.72	ND	ND	53	ND	1.29	4.92
93–0.025 μm	1.45	1.75	ND	1.8	65	0.066	1.28	5.61
93–0.22 μm	1.99	1.79	0.61	ND	77	0.068	1.34	5.61
96–10 kDa	0.79	1.23	0.34	2.8	45	0.064	1.20	ND
96–100 kDa	0.79	1.27	0.39	2.9	48	0.064	1.14	ND
96–0.22 μm	0.87	1.28	0.39	2.9	51	0.062	1.17	ND
96–2.5 μm	1.20	1.29	0.40	ND	57	0.071	1.33	ND
20–1 kDa	0.43	4.18	0.25	1.8	129	0.081	0.59	1.72
20–0.025 μm	0.55	4.61	0.43	1.7	141	0.086	0.75	3.22
20–0.22 μm	0.74	4.62	0.48	1.9	140	0.095	0.88	3.79
10–1 kDa	1.31	3.45	1.20	ND	59	0.093	1.63	4.77
10–0.025 μm	3.37	3.84	1.24	ND	119	0.080	1.85	5.70
10–0.22 μm	4.10	3.89	1.27	1.6	138	0.068	1.90	5.76

Element	Zn	Ga	Ge	As	Rb	Sr	Y	Zr
31–1 kDa	cntd	ND	0.007	0.11	0.07	13.6	0.063	0.068
31–0.025 μm	cntd	ND	0.007	0.12	0.07	15.1	0.527	0.716
31–0.22 μm	cntd	ND	0.015	0.14	0.07	16.9	0.613	0.935
31–5 μm	0.4	0.01	0.036	0.13	0.07	14.3	0.585	0.957
47–1 kDa	cntd	0.004	0.009	0.05	0.11	4.7	0.122	0.080
47–0.025 μm	cntd	0.013	0.011	0.06	0.14	8.0	0.659	0.801
47–0.22 μm	0.6	0.013	0.011	0.06	0.15	8.0	0.682	0.827
57–1 kDa	3.5	0.013	0.006	0.14	0.18	10.1	0.107	0.182
57–10 kDa	3.5	0.017	0.027	0.16	0.23	12.9	0.288	0.902
57–0.025 μm	3.6	0.025	0.075	0.19	0.23	14.2	0.452	1.437
57–0.22 μm	3.8	0.027	0.083	0.20	0.27	14.4	0.476	1.464
57–2.5 μm	3.8	0.030	0.073	0.19	0.27	14.9	0.487	1.535
57–5 μm	3.8	0.034	0.103	0.19	0.35	15.5	0.500	1.566
60–1 kDa	cntd	0.010	ND	0.11	0.09	13.4	0.068	0.069
60–10 kDa	cntd	0.011	ND	0.11	0.08	15.7	0.272	0.424
60–0.025 μm	cntd	0.014	ND	0.11	0.09	16.6	0.360	0.531
60–0.22 μm	0.4	0.015	ND	0.13	0.09	16.0	0.374	0.559
67–1 kDa	cntd	0.012	ND	0.12	0.11	16.3	0.108	0.166
67–10 kDa	cntd	0.012	ND	0.16	0.12	19.1	0.359	0.640
67–0.025 μm	cntd	0.013	ND	0.16	0.11	20.1	0.498	0.769
67–0.22 μm	0.57	0.013	ND	0.16	0.12	20.2	0.519	0.820
87–1 kDa	cntd	0.009	ND	0.14	0.14	15.6	0.355	0.562
87–10 kDa	cntd	0.010	ND	0.15	0.15	17.1	0.561	1.08
87–0.025 μm	cntd	0.011	ND	0.14	0.15	18.4	0.819	1.40
87–0.22 μm	1.17	0.014	ND	0.13	0.18	18.6	0.773	1.46

Table 1 (*continued*)

Element	Zn	Ga	Ge	As	Rb	Sr	Y	Zr
91–1 kDa	cntd	0.009	ND	0.10	0.14	17.6	0.133	0.195
91–10 kDa	cntd	0.010	ND	0.14	0.15	21.1	0.530	1.06
91–0.025 μm	0.52	0.012	ND	0.15	0.16	22.5	0.752	1.41
91–0.22 μm	0.49	0.015	ND	0.15	0.17	22.4	0.788	1.38
93–1 kDa	0.60	0.011	ND	0.13	0.10	20.3	0.193	0.346
93–10 kDa	0.71	0.012	ND	0.13	0.11	22.9	0.552	1.10
93–0.025 μm	0.71	0.012	ND	0.15	0.10	23.5	0.714	1.25
93–0.22 μm	0.75	0.013	ND	0.14	0.10	23.7	0.749	1.31
96–10 kDa	0.32	0.011	ND	0.13	0.11	27.5	0.500	0.593
96–100 kDa	0.36	0.012	ND	0.13	0.11	28.0	0.517	0.629
96–0.22 μm	0.36	ND	ND	0.13	0.11	28.0	0.546	0.608
96–2.5 μm	0.33	0.013	ND	0.13	0.11	28.1	0.541	0.656
20–1 kDa	1.48	0.031	ND	0.90	0.44	152	0.048	0.029
20–0.025 μm	1.44	0.031	ND	0.93	0.45	155	0.216	0.344
20–0.22 μm	2.19	0.035	ND	0.84	0.47	147	0.232	0.431
10–1 kDa	cntd	0.011	ND	0.28	0.13	70.7	0.399	0.905
10–0.025 μm	cntd	0.011	ND	0.31	0.15	78.2	1.00	1.97
10–0.22 μm	0.88	0.011	ND	0.28	0.11	75.6	0.901	2.17

Element	Mo	Ba	La	Ce	Pr	Nd	Sm	Eu
31–1 kDa	ND	0.271	0.014	0.012	0.003	0.017	0.004	0.001
31–0.025 μm	ND	0.299	0.101	0.135	0.033	0.169	0.050	0.013
31–0.22 μm	ND	0.267	0.105	0.146	0.037	0.183	0.058	0.016
31–5 μm	ND	0.291	0.119	0.170	0.042	0.204	0.058	0.017
47–1 kDa	<d.l.	0.092	0.022	0.030	0.008	0.038	0.010	0.003
47–0.025 μm	0.007	0.174	0.156	0.242	0.057	0.274	0.076	0.023
47–0.22 μm	0.012	0.180	0.166	0.255	0.058	0.284	0.078	0.023
57–1 kDa	0.056	0.582	0.020	0.032	0.006	0.029	0.008	0.003
57–10 kDa	0.074	0.756	0.044	0.084	0.015	0.077	0.022	0.006
57–0.025 μm	0.075	1.054	0.077	0.171	0.030	0.137	0.043	0.010
57–0.22 μm	0.070	1.128	0.084	0.187	0.030	0.149	0.043	0.012
57–2.5 μm	0.076	1.069	0.082	0.183	0.030	0.154	0.044	0.013
57–5 μm	0.087	1.567	0.079	0.189	0.030	0.144	0.044	0.012
60–1 kDa	ND	0.503	0.013	0.019	0.004	0.023	0.006	0.002
60–10 kDa	ND	0.555	0.069	0.101	0.023	0.112	0.034	0.005
60–0.025 μm	ND	0.691	0.106	0.146	0.034	0.157	0.041	0.012
60–0.22 μm	ND	0.637	0.113	0.164	0.038	0.173	0.047	0.012
67–1 kDa	ND	0.596	0.025	0.038	0.008	0.043	0.009	0.005
67–10 kDa	ND	0.596	0.097	0.145	0.031	0.149	0.037	0.009
67–0.025 μm	ND	0.599	0.144	0.209	0.046	0.215	0.056	0.017
67–0.22 μm	ND	0.580	0.162	0.235	0.049	0.235	0.060	0.016
87–1 kDa	ND	0.469	0.069	0.107	0.023	0.113	0.032	0.008
87–10 kDa	ND	0.472	0.126	0.188	0.041	0.206	0.056	0.013
87–0.025 μm	ND	0.522	0.214	0.322	0.071	0.331	0.091	0.020
87–0.22 μm	ND	0.553	0.204	0.312	0.067	0.319	0.084	0.023
91–1 kDa	ND	0.436	0.026	0.037	0.008	0.042	0.011	0.003
91–10 kDa	ND	0.445	0.124	0.180	0.041	0.197	0.052	0.013
91–0.025 μm	ND	0.476	0.199	0.286	0.063	0.300	0.082	0.021
91–0.22 μm	ND	0.505	0.221	0.309	0.069	0.326	0.091	0.020
93–1 kDa	0.036	0.376	0.036	0.048	0.012	0.057	0.016	0.005
93–10 kDa	0.032	0.420	0.115	0.158	0.037	0.184	0.050	0.016
93–0.025 μm	0.036	0.396	0.173	0.229	0.054	0.257	0.070	0.017
93–0.22 μm	0.033	0.392	0.169	0.242	0.055	0.264	0.073	0.021
96–10 kDa	<d.l.	0.465	0.116	0.184	0.038	0.187	0.052	0.015
96–100 kDa	<d.l.	0.434	0.118	0.191	0.038	0.197	0.054	0.014
96–0.22 μm	<d.l.	0.392	0.126	0.200	0.042	0.207	0.057	0.016
96–2.5 μm	<d.l.	0.426	0.127	0.203	0.042	0.208	0.057	0.015
20–1 kDa	0.021	1.63	0.017	0.009	0.002	0.011	0.003	0.001

(*continued on next page*)

Table 1 (*continued*)

Element	Mo	Ba	La	Ce	Pr	Nd	Sm	Eu
20–0.025 μm	0.027	1.55	0.041	0.043	0.012	0.068	0.020	0.005
20–0.22 μm	0.165	1.58	0.036	0.046	0.014	0.071	0.019	0.006
10–1 kDa	0.043	0.527	0.079	0.089	0.022	0.117	0.032	0.009
10–0.025 μm	0.067	0.478	0.207	0.272	0.068	0.330	0.101	0.028
10–0.22 μm	0.067	ND	0.203	0.276	0.067	0.325	ND	ND
Element	Gd	Tb	Dy	Ho	Er	Tm	Yb	Lu
31–1 kDa	0.007	0.001	0.008	0.002	0.008	0.001	0.009	0.001
31–0.025 μm	0.070	0.011	0.079	0.017	0.055	0.008	0.058	0.009
31–0.22 μm	0.082	0.014	0.091	0.021	0.068	0.010	0.066	0.012
31–5 μm	0.084	0.013	0.083	0.020	0.063	0.009	0.065	0.010
47–1 kDa	0.016	0.002	0.018	0.004	0.015	0.003	0.018	0.003
47–0.025 μm	0.095	0.017	0.109	0.024	0.077	0.012	0.076	0.012
47–0.22 μm	0.098	0.017	0.105	0.025	0.075	0.011	0.077	0.013
57–1 kDa	0.010	0.002	0.014	0.004	0.013	0.002	0.015	0.003
57–10 kDa	0.027	0.006	0.043	0.010	0.036	0.006	0.041	0.007
57–0.025 μm	0.056	0.010	0.070	0.017	0.056	0.009	0.062	0.010
57–0.22 μm	0.059	0.010	0.074	0.017	0.058	0.009	0.067	0.009
57–2.5 μm	0.058	0.011	0.075	0.019	0.060	0.009	0.066	0.011
57–5 μm	0.057	0.011	0.076	0.019	0.060	0.009	0.065	0.010
60–1 kDa	0.009	0.001	0.010	0.002	0.008	0.001	0.009	0.002
60–10 kDa	0.041	0.006	0.044	0.010	0.031	0.005	0.033	0.006
60–0.025 μm	0.055	0.008	0.059	0.013	0.039	0.006	0.042	0.006
60–0.22 μm	0.061	0.009	0.062	0.014	0.041	0.006	0.043	0.007
67–1 kDa	0.015	0.002	0.015	0.004	0.013	0.002	0.012	0.002
67–10 kDa	0.054	0.009	0.055	0.012	0.039	0.006	0.041	0.007
67–0.025 μm	0.071	0.012	0.077	0.017	0.053	0.008	0.053	0.009
67–0.22 μm	0.079	0.013	0.082	0.018	0.056	0.008	0.058	0.009
87–1 kDa	0.046	0.007	0.051	0.013	0.040	0.006	0.041	0.007
87–10 kDa	0.080	0.013	0.084	0.018	0.060	0.008	0.063	0.010
87–0.025 μm	0.119	0.019	0.125	0.029	0.086	0.013	0.087	0.015
87–0.22 μm	0.115	0.019	0.124	0.027	0.087	0.013	0.086	0.015
91–1 kDa	0.013	0.002	0.018	0.005	0.014	0.002	0.015	0.003
91–10 kDa	0.067	0.011	0.079	0.018	0.057	0.009	0.060	0.010
91–0.025 μm	0.112	0.018	0.117	0.026	0.081	0.012	0.083	0.013
91–0.22 μm	0.123	0.020	0.125	0.029	0.085	0.012	0.089	0.015
93–1 kDa	0.023	0.005	0.026	0.009	0.023	0.006	0.026	0.006
93–10 kDa	0.070	0.012	0.080	0.019	0.063	0.009	0.064	0.011
93–0.025 μm	0.094	0.016	0.108	0.024	0.079	0.012	0.085	0.014
93–0.22 μm	0.099	0.016	0.111	0.025	0.081	0.012	0.084	0.014
96–10 kDa	0.081	0.011	0.076	0.017	0.057	0.007	0.054	0.008
96–100 kDa	0.085	0.013	0.082	0.017	0.060	0.007	0.058	0.008
96–0.22 μm	0.093	0.012	0.088	0.018	0.058	0.008	0.061	0.009
96–2.5 μm	0.090	0.013	0.087	0.018	0.060	0.008	0.059	0.008
20–1 kDa	0.005	0.000	0.006	0.001	0.004	0.000	0.005	0.000
20–0.025 μm	0.028	0.004	0.031	0.006	0.023	0.002	0.025	0.003
20–0.22 μm	0.029	0.005	0.031	0.007	0.022	0.003	0.022	0.004
10–1 kDa	0.051	0.008	0.055	0.014	0.044	0.007	0.049	0.008
10–0.025 μm	0.146	0.022	0.153	0.034	0.112	0.017	0.116	0.019
10–0.22 μm	ND	ND	ND	ND	ND	ND	ND	ND
Element	Pb	Th	U					
31–1 kDa	0.005	0.000	0.001					
31–0.025 μm	0.048	0.005	0.005					
31–0.22 μm	0.056	0.012	0.006					
31–5 μm	0.061	0.012	0.007					
47–1 kDa	0.013	0.001	0.002					
47–0.025 μm	0.034	0.021	0.012					
47–0.22 μm	0.034	0.021	0.013					

Table 1 (*continued*)

Element	Pb	Th	U
57–1 kDa	0.004	0.001	0.001
57–10 kDa	0.047	0.007	0.002
57–0.025 μm	0.068	0.014	0.002
57–0.22 μm	0.066	0.014	0.002
57–2.5 μm	0.065	0.015	0.003
57–5 μm	0.069	0.015	0.003
60–1 kDa	0.005	<d.l.	0.001
60–10 kDa	ND	0.006	0.005
60–0.025 μm	ND	0.008	0.006
60–0.22 μm	0.006	0.009	0.006
67–1 kDa	ND	0.001	0.003
67–10 kDa	ND	0.009	0.007
67–0.025 μm	ND	0.014	0.008
67–0.22 μm	0.009	0.015	0.009
87–1 kDa	0.031	0.004	0.009
87–10 kDa	0.044	0.012	0.013
87–0.025 μm	0.048	0.020	0.018
87–0.22 μm	0.043	0.020	0.017
91–1 kDa	0.014	<d.l.	0.003
91–10 kDa	0.013	0.011	0.011
91–0.025 μm	0.012	0.015	0.014
91–0.22 μm	0.022	0.017	0.014
93–1 kDa	ND	0.004	0.006
93–10 kDa	ND	0.011	0.016
93–0.025 μm	ND	0.013	0.018
93–0.22 μm	0.004	0.014	0.019
96–10 kDa	ND	0.003	0.011
96–100 kDa	ND	0.003	0.012
96–0.22 μm	0.006	0.004	0.012
96–2.5 μm	ND	0.004	0.012
20–1 kDa	0.031	ND	0.022
20–0.025 μm	0.033	ND	0.028
20–0.22 μm	0.035	0.003	0.028
10–1 kDa	ND	0.006	0.013
10–0.025 μm	ND	0.021	0.027
10–0.22 μm	0.011	0.023	0.027

cntd means contamination and ND stands for non-determined. All concentrations are in μg/L.

BE-N, LKSD-1, SRM 1515 and the recommended values was obtained producing a relative difference <10% for all certified elements. The uncertainty on non-certified elements (i.e., Tl for BE-N and LKSD-1; Ti, Bi, Tl, Ta, Hf, Dy, Tb, Lu for SRM 1515) cannot be assessed but estimated from the internal reproducibility of our analysis as 20–30%.

3. Results and discussion

3.1. Concentration and size fractionation of chemical elements

3.1.1. Major elements

Dissolved (<0.22 μm) concentrations of major elements in all rivers, soil solutions and groundwaters (suprapermafrost flow) together with collection procedure are presented in the previous work (Pokrovsky et al., 2005b) whereas the results of the ultrafiltration experiments are listed in Table 1. Dissolved (<0.22 μm) concentrations of all TE in soil porewaters, groundwater and rivers are given in the Electronic Annex. The studied waters are essentially neutral with pH varying from 6.7 to 7.7. No difference was detected between pH values of filtrates and ultrafiltrates within ±0.10 pH units. All rivers exhibit high concentrations of dissolved (<0.22 μm) organic carbon (DOC), ranging from 10 to 30 mg/L, which is typical for rivers draining boreal peatlands (Gordeev et al., 1996; Ingri et al., 2000; Millot et al., 2003). The inorganic charge ($i = (\sum^{+} - \sum^{-})/\sum^{+}$) for rivers having <15 mg/L of OC varies from 0 to 20%. For organic-rich rivers and soil solutions ((OC) = 20–30 mg/L), i achieves 30–40% being positively correlated with (OC).

Typical OC distribution among filtrates of various pore sizes are shown in Fig. 2. Usually, more than 90% of 0.22 μm-filter passed OC is concentrated in <10 kDa fraction and 70–90% of OC passes through 1-kDa membrane. All soil porewaters, groundwaters (suprapermafrost flow) and small, medium and large rivers exhibit ultrafiltration OC patterns, similar to that of granitic boreal rivers (Pokrovsky and Schott, 2002; Ingri et al., 2004), but different

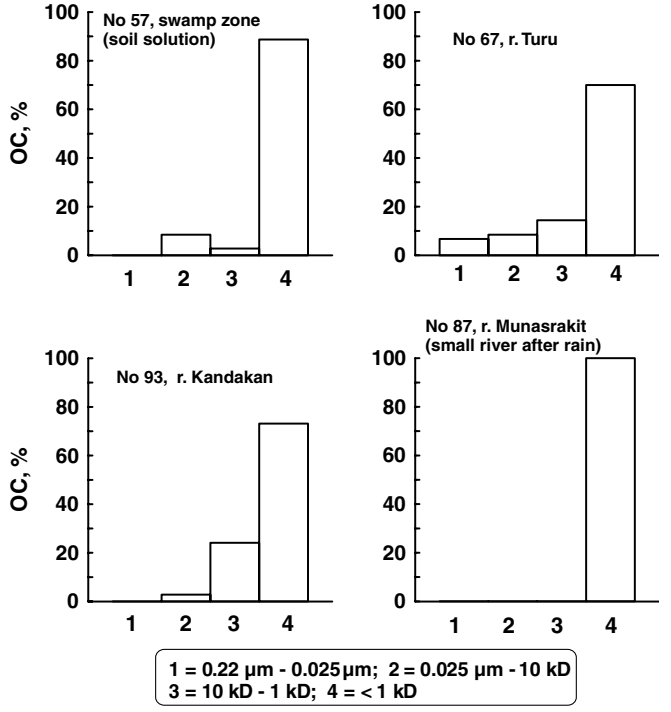

Fig. 2. Stack diagram of OC distribution in various fractions of filtered and ultrafiltered samples.

from that of tropical rivers (Viers et al., 1997) and temperate peat and podzol soil solutions (Pokrovsky et al., 2005a) where the proportion of large-size organic colloids (10 kDa to 0.22 μm) can be as high as 60%. A possible explanation for this observation is that in cold boreal regions, slow degradation of fresh plant litter does not allow formation of long polymerized humic chains. Consequently, low molecular weight (LMW) organic matter represents most of the dissolved organics in surficial fluids. Indeed, it is known that for northern Siberian soils the litter decomposition occurs slowly (Trumbore and Harden, 1997), whereas the abundant precipitation during summer leads to fast leaching of all degradation products and formation of so-called "aggressive" (low-polymerized) dissolved organic matter of a fulvic nature that moves downward through the soil profile (Rode, 1937; Kononova, 1963; Targulian, 1971).

Concentration of iron and aluminum, unlike DOC, strongly decreases during the ultrafiltration. Fe and Al are present in the form of large-size colloids (0.22 μm to 10 kDa) and they are essentially removed from solution before the filtration through 10 and 1 kDa membranes, as only 10–30% of these metals is concentrated in <1 kDa fraction. In river samples, Fe concentrations do not exceed 200 μg/L and that of Al is a factor of 2 lower. In the swamp soil solutions, however, Fe and Al concentrations reach 1–1.5 mg/L, typical for wetland peat areas (Pokrovsky et al., 2005a). Soil solutions exhibit much higher variation of [Fe] and [Al] in 0.22 μm filtrates but follow the same general trend as small and medium rivers and groundwaters. A linear correlation between [Al] and [Fe] is observed in all UF experiments ($0.9 < R^2 < 0.99$, Fig. 3), suggesting that iron and aluminum

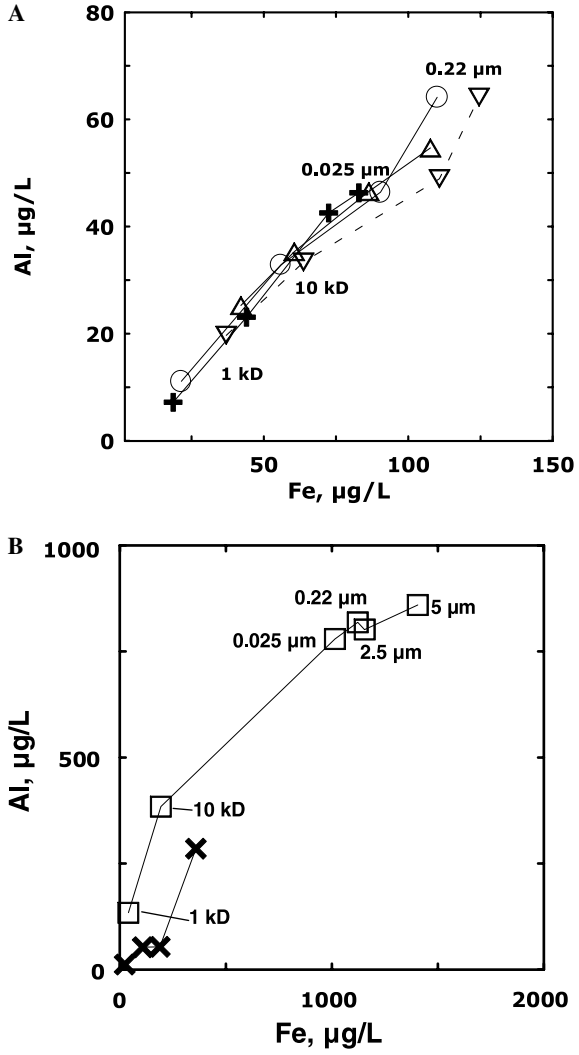

Fig. 3. Correlation between Fe and Al in various filtrates ($0.9 \leqslant R^2 \leqslant 0.99$). (A) Rivers, low concentration of metals; (B) Swamp waters, high concentration of metals. The significance of the symbols is the following—○: No. 91, river Culkan; ♦: No. 47, Soil porewater; □: No. 57, Swamp water; ✖: No. 31, river Razebaika; ✚: No. 60, river Korvunchana; △: No. 67, river Turu; ▽: No. 87, river Munasrakit; ◁: No. 93, river Kandakan; ✳: No. 10, river Khenochangda. For each filtration experiment, the first (upper) symbol corresponds to 5 or 0.22 μm pore size and the last (lower) one corresponds to 1 kDa. Solid connecting lines are for guiding purposes.

exhibit the same size distribution. For simplicity, we will use iron concentration as an index of colloid abundance.

Among major elements, dissolved silica concentration is the least influenced by ultrafiltration: within the analytical uncertainty of 2%, we have not found any difference between Si concentration in various filtrates, from 5 μm to 1 kDa (Table 1). This indicates the absence of small-size phytolites, clays or silica-rich organic debris in these waters and confirms that the major part of aqueous silica is not associated with colloids.

3.1.2. Elements exhibiting <30–50% differences between filtrates

Alkalis and alkali-earth elements are mostly present in the dissolved phase. Concentrations of all major cations

(Na, Mg, K, Ca) and trace elements (Li, Rb, Cs, Sr, Ba) do not change by more than 10–20 % between the size fraction from 10 kDa to 1 kDa. Concentrations of Ni, Co, Cr, Cu and Zn (from 0.2 to 6 μg/L) are within the range reported for large rivers such as the Mackenzie, Mississippi, Amazon, Ob, Yenisei and Lena Rivers and close to the world average values (Gaillardet et al., 2003). Concentrations of Cu, Ni, Cr and Co decrease by 30–50% upon ultrafiltration from 0.025 μm or 10 kDa to 1 kDa (Table 1) suggesting an important role of small-size colloids or organic complexes. Manganese and Zn concentrations do not vary by more than 20% between the filtrates implying both are truly dissolved or form <1 kDa organic complexes. In most of the studied surficial waters, dissolved Pb concentrations (from 0.01 to 0.05 μg/L) are similar to those reported in the Ob, Yenisei and Lena Rivers (Martin et al., 1993; Dai and Martin, 1995). Lead concentration variations between filtrates could be detected only in Fe-organic-rich peat swamp zone (No. 57, Table 1). In this sample, the Pb concentration decreases tenfold from 10 kDa to 1 kDa, suggesting, in accord with literature data (Erel et al., 1991), that colloids control Pb concentration in Fe-rich waters.

The ranges of V, As, Se, Nb, Mo, Sn and Sb concentrations (0.5–5 μg/L, 0.1–0.3 μg/L, 0.1–0.5 μg/L, 0.001–0.01 μg/L, 0.01–0.2 μg/L, 0.01–0.1 μg/L and 0.02–0.2 μg/L, respectively) in <0.22 μm fractions are similar to those reported for organic-rich tropical (Konhauser et al., 1994; Viers et al., 1997) and granitic boreal rivers (Johannesson et al., 2000; Pokrovsky and Schott, 2002). None of these elements exhibit a clear correlation with dissolved Fe or DOC in 0.22 μm filtrates and ultrafiltrates ($R^2 < 0.5$). Even in the organic- and Fe-rich soil water solutions from the swamp zones (No. 57, [Fe] = 1.1 mg/L; [OC] = 28 mg/L), concentrations of all elements, except V, remain constant between filtrates. At the neutral pH values encountered in most samples and under well oxygenated conditions, these elements are likely to be present in the form of oxyanions or neutral molecules whose interaction with mineral colloids is hampered by The negative charge of OM (i.e., Wilkinson et al., 1997).

3.1.3. Elements exhibiting large differences (>50%) between filtrates

Trivalent, tetravalent elements and uranium exhibit strong affinity for the colloidal fraction in sampled waters. Between 30 and 50% of gallium and 80–90% of yttrium are concentrated in >1 kDa fraction and their concentration decreases linearly with that of Fe ($0.8 \leqslant R^2 \leqslant 0.98$). La and Ce concentrations in sampled fluids range from 0.05 to 0.5 μg/L in <0.22 μm fraction, which is similar to the values reported for tropical (Dupré et al., 1996; Viers et al., 1997), temperate (Johannesson et al., 2004) and boreal (Lahermo et al., 1995; Ingri et al., 2000; Pokrovsky and Schott, 2002; Millot et al., 2003) organic-rich circum-neutral rivers. Typically, more than 80% of REEs is concentrated in >1 kDa fraction. This is consistent with well-known properties of REE to be associated with river colloids (Sholkovitz, 1992). From large to smaller poresizes, their concentrations gradually decrease in proportion to those of Fe or Al ($0.9 \leqslant R^2 \leqslant 0.99$) suggesting strong control of mineral colloids on REE concentrations (Figs. 4A and B). Heavy REE (HREE) exhibit a higher affinity for small size colloids and the "truly dissolved" <1 kDa fraction. This is illustrated in Fig. 4C where the ratio of [La]/[Yb] measured in various ultrafiltrate fractions is plotted as a function of Fe concentration. This ratio increases by a factor of 2 for size fractions from 1 kDa to 0.22 μm. This agrees with general tendency of light REE (LREE) to form adsorbed complexes on inorganic phases (oxides) and HREE to form stronger aqueous complexes with organic ligands (Sholkovitz, 1995; Sonke and Salters, 2006) or with carbonate ions (Tang and Johannesson, 2003). Indeed, the REE pattern of ultrafiltrate (<1 kDa) to filtrate (<0.22 μm) ratio in small creek Munasrakit (No. 87) and soil solution (No. 47) exhibits a rise towards HREE (Fig. 4D). All studied samples (large and small rivers, groundwaters and soil porewaters) exhibit very similar upper-crust normalized REE patterns.

The dominant role of mineral colloids in Ti chemical status in solution is revealed by the ultrafiltration procedure: a good positive correlation is observed between [Ti] and [Fe] ($0.93 \leqslant R^2 \leqslant 0.99$) in filtrates and ultrafiltrates of small and large rivers, groundwaters and soil porewaters at "low" (i.e., <200 μg/L, Fig. 5) and high (i.e., <1500 μg/L for samples Nos. 31 and 57, not shown) dissolved Fe concentrations. In most ultrafiltrates, there is no dependence between [Ti] and [OC] as with decrease of the filter poresize, [Ti] decreases by a factor of 10, but [OC] remains constant or changes by not more than 20–30% (Table 1).

In most studied rivers, the Ge concentration is extremely low (0.01–0.005 μg/L) and comparable with the world average (Gaillardet et al., 2003). Only in the Fe and OC-rich soil solution of the swamp zone (No. 57), and in the river issuing from the wetland territory (No. 31), were measurable concentrations of Ge found. In ultrafiltrates of these samples, Ge and Fe (or Al) concentrations are well correlated ($R^2 = 0.99$) suggesting primary control by mineral colloids. At the same time, in sample Nos. 31 and 57, [Ge] exhibits no dependence on [OC].

Dissolved (<0.22 μm) Zr, Hf and Th concentrations vary from 0.5 to 2 μg/L, 0.01 to 0.05 μg/L and 0.005 to 0.03 μg/L, respectively, being correlated both with [Fe] and [Al] ($0.8 \leqslant R^2 \leqslant 0.99$), but not [OC] (no dependence). The <0.22 μm concentrations are tenfold higher than the average values for world rivers (Gaillardet et al., 2003) but close to those reported in organic-rich tropical waters of Cameroon (Dupré et al., 1996; Viers et al., 1997) and boreal streams from the Karelian region (Pokrovsky and Schott, 2002). Similar to Ti and Ge, no difference in Zr, Hf and Th concentrations were found between large and small rivers, groundwaters and soil solutions. The ultrafiltration procedure demonstrates that the size distribution of these elements is fully controlled by >1 kDa colloids (Figs. 6A and B).

Uranium exhibits similar <0.22 μm concentration ranges (i.e., 0.006–0.03 μg/L) among large and small rivers,

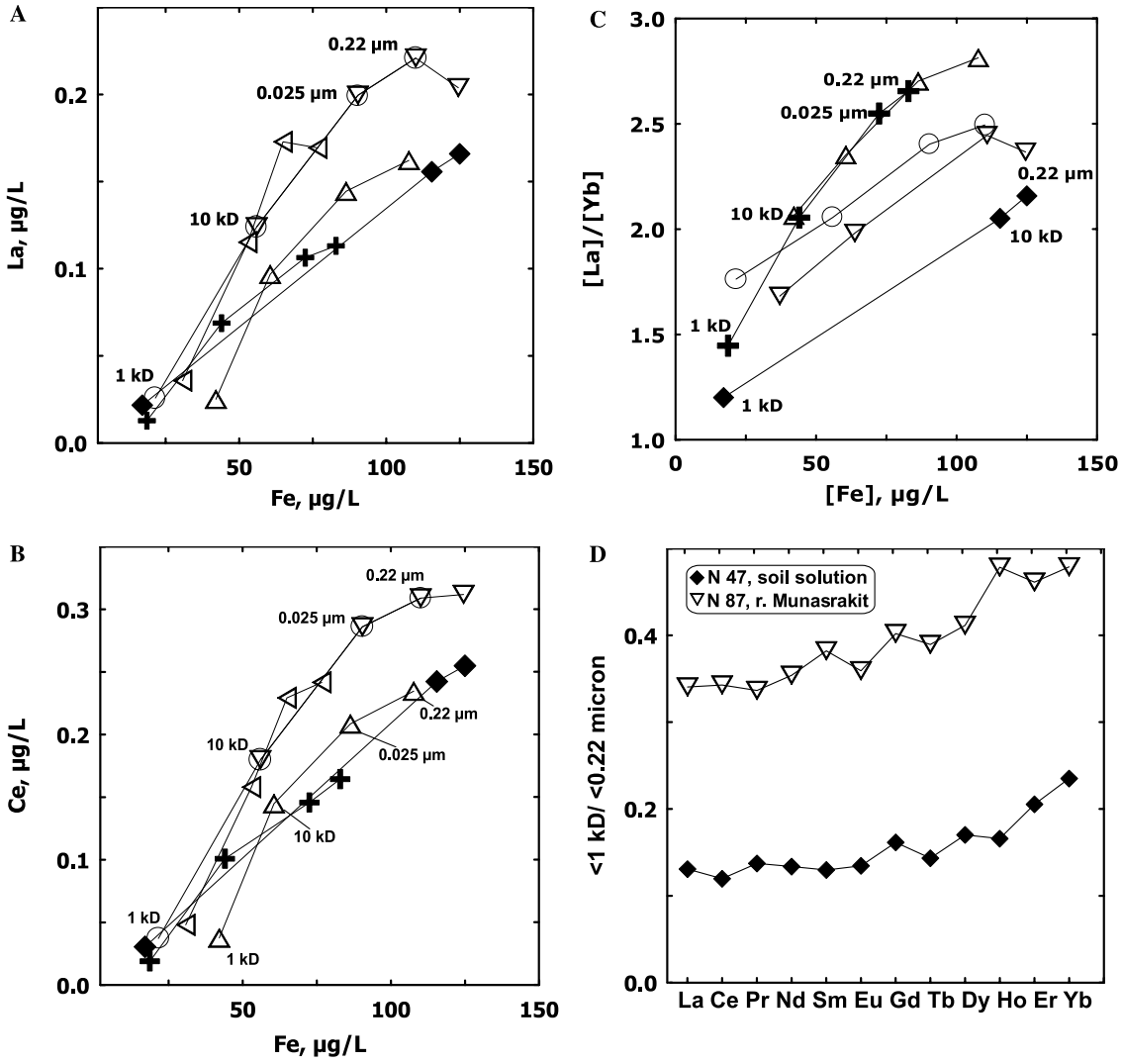

Fig. 4. Lanthanum (A) and cerium (B) concentration as a function of Fe concentration in successive filtrates from 0.22 μm to 1 kDa ($0.9 \leqslant R^2 \leqslant 0.99$). The significance of the symbols is the following—○: No. 91, river Culkan; ♦: No. 47, Soil porewater; ✚: No. 60, river Korvunchana; : △: No. 67, river Turu; ▽: No. 87, river Munasrakit; ◁: No. 93, river Kandakan. For each filtration experiment, the first (upper) symbol corresponds to 0.22 μm pore size and the last (lower) one corresponds to 1 kDa. Solid connecting lines are for guiding purposes. (C) Concentration ratio [La]/[Yb] as a function of [Fe] in the ultrafiltrates. The significance of the symbols is the same as for (A) and (B). The solid lines are for guiding purposes. (D) REE pattern of ultrafiltrate (<1 kDa) to filtrate (<0.22 μm) ratio in river and soil solution.

groundwaters, permafrost and soil solutions. These values are much lower than the world average (0.37 μg/L, Gaillardet et al., 2003) but comparable to the data of silicate-draining organic-rich tropical and boreal rivers (Palmer and Edmond, 1993; Porcelli et al., 1997; Viers et al., 1997). Transport of U by organic colloids in boreal rivers demonstrated by Porcelli et al. (1997) for granitic watersheds is not seen in our study as no dependence between [OC] and [U] is observed in ultrafiltrates. In contrast, strong correlations ($0.8 < R^2 < 0.95$) between iron (or aluminum) and uranium concentrations exist in the ultrafiltrates (Fig. 7), suggesting the important role of mineral colloids in U transport in soil solutions and surface waters. On average, more than 50% of U is present in >1 kDa fraction.

3.1.4. Thermodynamic considerations

We assessed elements speciation using the MINTEQA2 computer code (Allison et al., 1991) with an implemented database for binding of metals to discrete carboxylic sites (Allison and Perdue, 1994). This calculation has been performed assuming a constant content of 10 μeq COO^- per mg DOC (Oliver et al., 1983). At the pH value of most <0.22 μm filtered samples investigated in this study (7.0 ± 0.5), undersaturation of solutions with respect to insoluble solid phase (oxides, oxy(hydr)oxides, carbonates, phosphates) is predicted for Ti, $VO_2(OH_2)^-$, Cr(III) and CrO_4^{2-}, Co, Ni, Cu, Zn, Mn, Mo, As, Sb, Sn, As, Cd, Pb, Ge, U, Ga, Y, REE based on solubilities and stability constants given in Baes and Mesmer (1976) and Martell et al. (1997). The fluids are supersaturated with respect to

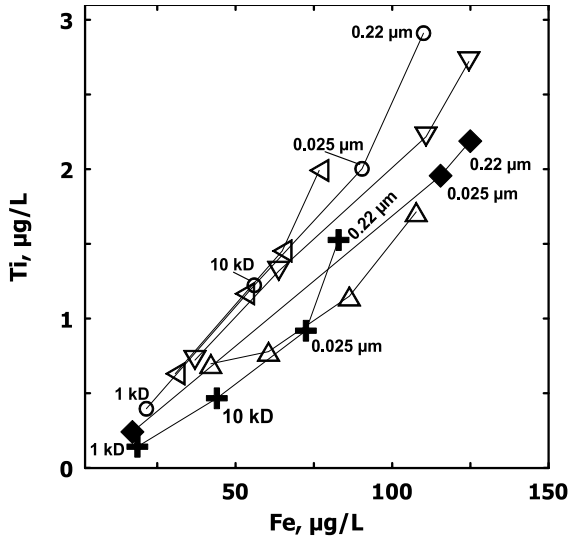

Fig. 5. Fe–Ti concentration dependence in the ultrafiltrates ($0.93 \leqslant R^2 \leqslant 0.99$). The significance of the symbols symbols is the following—○: No. 91, river Culkan; ♦: No. 47, Soil porewater; ✚: No. 60, river Korvunchana; △: No. 67, river Turu; ▽: No. 87, river Munasrakit; ◁: No. 93, river Kandakan; For each filtration experiment, the first (upper) symbol corresponds to 0.22 µm pore size and the last (lower) one corresponds to 1 kDa. Solid connecting lines are for guiding purposes.

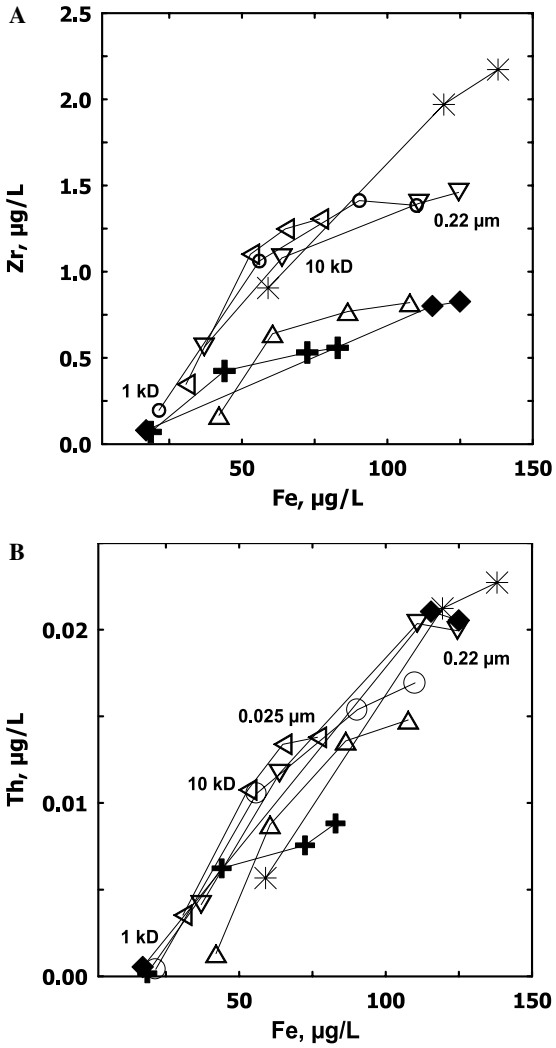

Fig. 6. Zr–Fe (A) and Th–Fe (B) correlation in the ultrafiltrates ($0.8 \leqslant R^2 \leqslant 0.99$). The significance of the symbols is the following—○: No. 91, river Culkan; ♦: No. 47, Soil porewater; ✖: No. 31, river Razebaika; ✚: No. 60, river Korvunchana; △: No. 67, river Turu; ▽: No. 87, river Munasrakit; ◁: No. 93, river Kandakan; ✳: No. 10, river Khenochangda. For each filtration experiment, the first (upper) symbol corresponds to 5 or 0.22 µm pore size and the last (lower) one corresponds to 1 kDa. Solid connecting lines are for guiding purposes.

gibbsite, ferrihydrite, goethite and oxy(hydr)-oxides of Th, Zr and Hf.

In order to distinguish between adsorption of TE on the surface of colloids and coprecipitation, we estimated the surface area of colloids in each filtrate following the method described earlier by Pokrovsky and Schott (2002) and Pokrovsky et al. (2005a). Assuming that the typical abundance of metal- and anion-available surface site for iron or aluminum oxides is 3 µmol/m^2 (Dzombak and Morel, 1990), the average concentration of available surface sites for most samples (0.2–0.6 µmol/L) is comparable with the total TE concentration in <0.22 µm—filtered solutions (i.e., ~0.1–0.2 µmol/L). This suggests that the overall surface area of mineral colloids is sufficient to adsorb all trace elements present in >1 kDa fraction. However, the number of surface sites in large-size colloids (10 kDa to 0.22 µm) represents only $1 \pm 0.5\%$ of the total available sites, whereas they retain more than half of many TE (Ti, Zr, Hf, Ga, Y, REEs). This implies the preferential incorporation of TE in the bulk of large colloids via coprecipitation rather than sorption on colloid surfaces. For quantitative assessment of the parameters of this process, we calculated the iron-normalized TE partition coefficient between dissolved (<1 kDa) and colloidal (1 kDa to 0.22 µm) fractions defined as

$$K_d = (\mathrm{TE/Fe})_{\mathrm{colloidal}}/(\mathrm{TE/Fe})_{\mathrm{dissolved}}.$$

Iron-normalized K_d values range from 0.2–0.3 to 1–2 (Table 2). These values are highest for trivalent and tetravalent elements: Ti (1.6–0.9), Zr (1.6–1.2), Y and REEs (0.8–2.0). Note a systematic decrease of K_d from La and Ce to Yb and Lu in agreement with the tendency of LREEs to adsorb/coprecipitate with Fe hydroxide and HREE to form stable aqueous complexes in solution (see Figs. 4C and D). The value of K_d for Ge (0.5) assessed from a sole sample of swamp water (No. 57) is comparable with $K_d = 0.7$–0.9 obtained in the laboratory (Pokrovsky et al., 2006). Highly soluble elements exhibiting only weak affinity for colloids (V, Mn, Co, Ni, Cu, Zn, As, Mo, Sn, Sb, Section 3.1.2) have K_d values between 0.05 and 0.3.

The chemical nature of iron/aluminum colloids formed in organic-rich surficial waters is not well known. Using a set of spectroscopic techniques (Electronic Paramagnetic Resonance, Infrared Spectroscopy) Olivié-Lauquet et al. (1999) showed that Fe(III) dominates the colloidal material from Cameroon rivers both as organic complexes and

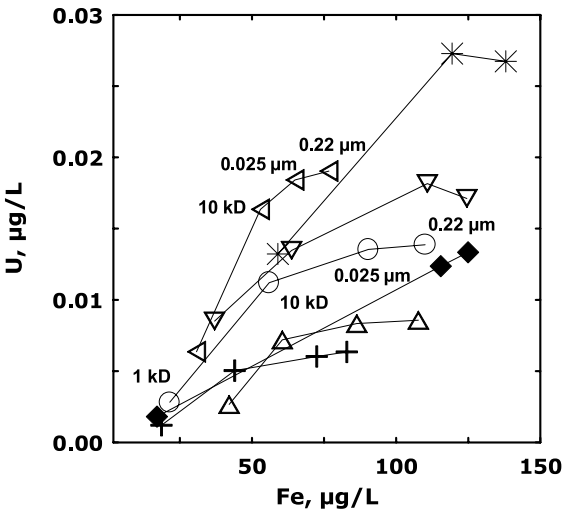

Fig. 7. Uranium concentration as a function of Fe concentration in successive filtrates from 0.22 µm to 1 kDa ($0.8 < R^2 < 0.95$). The significance of the symbols is the following—○: No. 91, river Culkan; ♦: No. 47, Soil porewater; ✚: No. 60, river Korvunchana; △: No. 67, river Turu; ▽: No. 87, river Munasrakit; ◁: No. 93, river Kandakan; ✳: No. 10, river Khenochangda. For each filtration experiment, the first (upper) symbol corresponds to 5 or 0.22 µm pore size and the last (lower) one corresponds to 1 kDa. Solid connecting lines are for guiding purposes.

inorganic (hydr)oxides and that the proportion of Fe inorganic colloids in organic-rich waters is generally underestimated. Allard et al. (2004) argued that colloidal forms of iron in rivers of the Amazon Basin are represented by iron oxides and Fe^{3+} bound to organic matter. Amorphous iron hydroxide whose large sorptive and coprecipitation capacities are well known thus can serve as important TE carriers both in organic-rich tropical (Olivié-Lauquet et al., 2000), temperate (Gordeev et al., 2004) rivers and DOC-poor groundwaters (Dia et al., 2000). Important role of humic organic matter on Fe(III) oxy(hydr)oxide colloid stabilization in rivers and groundwaters has been demonstrated by spectroscopic and macroscopic techniques (Rose et al., 1998; Schafer et al., 2003a,b; Lyvén et al., 2003).

3.2. Dissolved and particulate fluxes of TE

Based on chemical analysis of Kochechumo river suspended matter (RSM-1), the mean annual fluxes of TE in particulate and dissolved forms were calculated for Putorana rivers (Table 3) assuming that: (i) average dissolved (<0.22 µm) concentrations of TE in 60 rivers during summer can serve as an approximation (±30–50%) for mean annual values (this is true for major elements, see Pokrovsky et al., 2005b); and (ii) the TE composition of Kochechumo river suspended matter, which is very close to that of the soil clay fraction, is representative for all rivers of the region. To derive the RSM fluxes, we used the mean multi-annual values of the Russian Hydrological Survey for the Taimura River (Pokrovsky et al., 2005b). The stack diagram of the proportion of TE transport in the dissolved phase is presented in Fig. 8.

Table 2
K_d values for TE distribution between dissolved (<1 kDa) and colloidal (1 kDa–0.22 µm) phase

Sample	Ti	V	Cr	Co	Ni	Cu	Ga	Ge	Y	Zr	La	Ce	Pr	Nd
N 31	0.80	0.02	0.2	0.1	0.2	0.3	ND	ND	1.2	1.8	0.9	1.5	1.6	1.4
N 47	1.30	0.10	1.3	0.2	0.2	0.2	0.3	ND	0.7	1.5	1.0	1.2	1.0	1.0
N 57	0.55	0.06	0.04	0.04	0.03	0.02	0.04	0.50	0.13	0.26	0.12	0.18	0.14	0.15
Avg. wetlands	0.86	0.05	0.54	0.12	0.15	0.19	0.17		0.68	1.16	0.69	0.94	0.92	0.85
N 60	2.90	0.08	0.37	0.05	0.22	0.26	0.15	ND	1.3	2.09	2.33	2.28	2.37	1.89
N 67	0.93	0.12	0.82	0.06	0.71	0.69	0.03	ND	2.4	2.52	3.50	3.36	3.15	2.86
N 87	1.17	0.06	0.19	0.23	0.15	0.18	0.23	ND	0.50	0.68	0.82	0.81	0.83	0.77
N 91	1.54	0.03	0.14	0.17	0.18	0.25	0.15	ND	1.20	1.48	1.84	1.77	1.83	1.64
N 93	1.42	0.13	ND	ND	0.22	0.53	0.13	ND	1.90	1.83	2.47	2.65	2.42	2.37
N 10	1.60	0.10	0.04	ND	0.13	0.16	0.03	ND	0.94	1.05	1.18	1.57	1.49	1.32
Avg. rivers	1.6	0.09	0.31	0.13	0.25	0.3	0.12		1.4	1.6	2.0	2.1	2.0	1.8

Sample	Sm	Eu	Gd	Tb	Dy	Ho	Er	Tm	Yb	Lu	Pb	Th	U
N 31	1.9	1.4	1.5	1.7	1.5	1.3	1.1	1.0	1.1	1.0	1.6	2.7	0.5
N 47	1.1	1.0	0.8	0.9	0.8	0.8	0.6	0.5	0.5	0.5	0.3	5.9	1.0
N 57	0.16	0.13	0.18	0.16	0.15	0.13	0.128	0.099	0.12	0.085	0.50	0.48	0.04
Avg. wetlands	1.05	0.83	0.84	0.93	0.82	0.73	0.613	0.538	0.57	0.53	0.78	3.03	0.52
N 60	2.07	1.17	1.65	1.59	1.58	1.55	1.18	1.33	1.14	1.05	0.02	14.5	1.27
N 67	3.72	1.26	2.74	2.76	2.89	2.49	2.22	1.73	2.40	1.83	ND	6.56	1.42
N 87	0.68	0.76	0.63	0.66	0.61	0.46	0.49	0.46	0.46	0.45	0.17	1.62	0.43
N 91	1.80	1.35	2.11	1.83	1.46	1.18	1.24	1.01	1.23	1.05	0.16	9.92	0.95
N 93	2.31	2.32	2.21	1.58	2.16	1.20	1.65	0.739	1.51	0.94	ND	1.92	1.31
N 10	ND	ND	ND	ND	ND	ND	ND	ND	ND	0.91	ND	2.25	0.76
Avg. rivers	2.1	1.4	1.9	1.7	1.7	1.4	1.4	1.1	1.3	1.0	0.11	6.1	1.0

ND = non-determined.

Table 3
Mean annual fluxes of TE in suspended and dissolved forms for Taimura river

	Suspended flux, g/km^2/y	Dissolved concentration, mg/t	Dissolved flux, g/km^2/y
B	13.4	8.800	1,800
Li	22	0.310	672
V	821	1.89	387
Cr	517	0.61	125
Mn	3745	2.02	414
Co	97	0.08	16
Ni	252	1.29	264
Cu	193	5.06	1,040
Zn	288	2.53	519
As	3.0	0.17	35
Se	11.5	0.22	45
Rb	34.1	0.14	80
Sr	621	37	31,400
Y	67.6	0.55	113
Zr	246	1.12	223
Mo	1.0	0.042	8.6
Cd	0.4	0.0062	1.3
Sn	2.4	0.022	4.5
Sb	0.2	0.02	4.1
Ba	438	0.6	123
La	20.9	0.123	25
Ce	49.5	0.19	39
Nd	32.7	0.21	43
Yb	7.3	0.067	14
Hf	7.2	0.025	5.1
Pb	7.7	0.022	4.5
Th	3.3	0.013	2.7
U	0.9	0.016	3.3

Several groups of elements can be distinguished: (i) those exhibiting high mobility in weathering processes (60–90% of total element flux is in dissolved form) because of high solubility of their mineral phases, weak adsorption/complexation with organic and mineral colloids and low concentrations in minerals common to basaltic rocks (B, Sr, Li, Sb, As, Mo, Se, Rb, Sn); (ii) transition metals having 50–80% of flux in the <0.22 μm form and likely present in mobile, low-molecular weight (<1–10 kDa) organic complexes (Cu, Zn, Ni); and (iii) normally "immobile" trace elements having 40–80% of their annual flux in the dissolved form and exhibiting high affinity for organo-mineral Fe–Al colloids (Pb, Y, REEs, U, Zr, Hf, Th). Some soluble elements (Ba, V, Cr, Co, Mn) exhibit weaker transport in solution (dissolved flux <30%) compared to suspended solids because of their elevated concentrations in rocks, soil and residual minerals and RSM. Finally, Ti, Fe and Al are essentially transported in the solid phase because of their high concentration in the RSM.

Assuming aluminum is mostly immobile during weathering (Polynov, 1944; Chesworth et al., 1981), one can compare the aluminum-normalized elemental ratios of various solid reservoirs with those of basalt (Fig. 9). Most Al-normalized trace element concentrations in soils and suspended matter samples are the same as in basalts (1.0 ± 0.1). The deep and subsurface soil horizons (samples 17a, 71b) exhibit similar features, being slightly enriched in Cs, As, Ba, Cd, W, Ta, Tl, Bi. Bearing in mind typical uncertainties of 10–30% related to TE content variations in basalts (Zolotukhin and Al'Mukhamedov, 1988), this implies that basalt weathering in Central Siberia does not appreciably fractionate elements. Similar conclusions have been reached for chemical erosion products of basic rocks in tropical and temperate climates (Louvat and Allégre, 1997, 1998). Preferential release of the most soluble elements (i.e., Na, Ca, Mg, Sr, Rb, Ba, U) during rock dissolution reported for large world river basins (i.e., Dupré et al., 1996) is not observed for Siberian basalts. Enrichment in Cs and Pb of soils and suspended matter compared to basalts was also reported for rivers of the Azores (Louvat and Allégre, 1998). Plant litter and the upper organic-rich soil horizon exhibit the highest variations of (TE/Al) compared to original basalt.

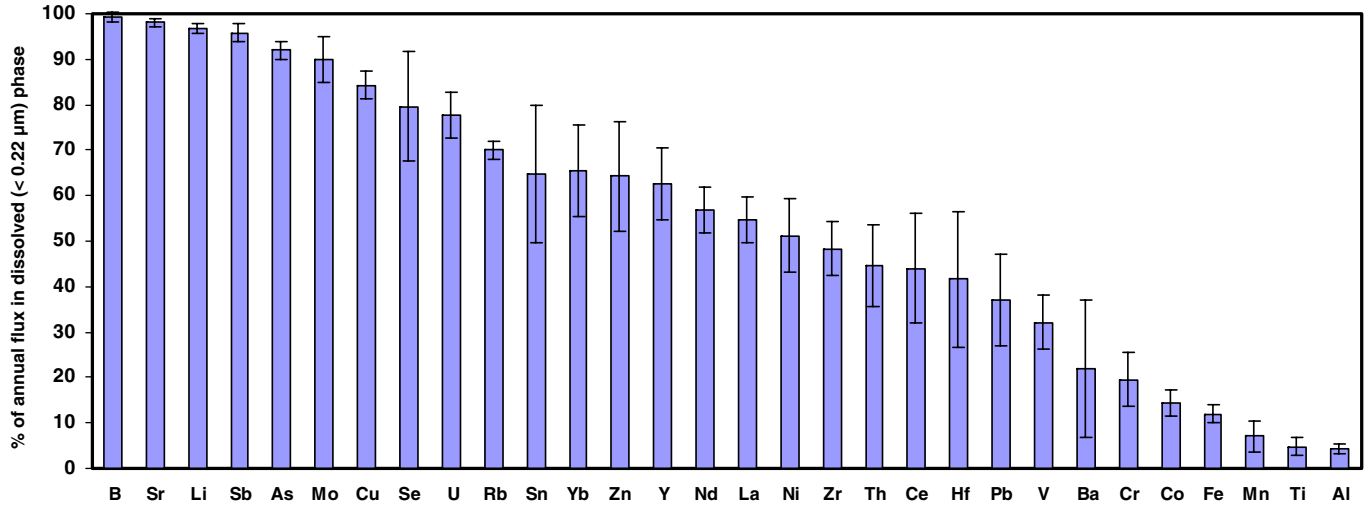

Fig. 8. Percentage of annual flux in dissolved (<0.22 μm) phase for trace elements in rivers of Central Siberia.

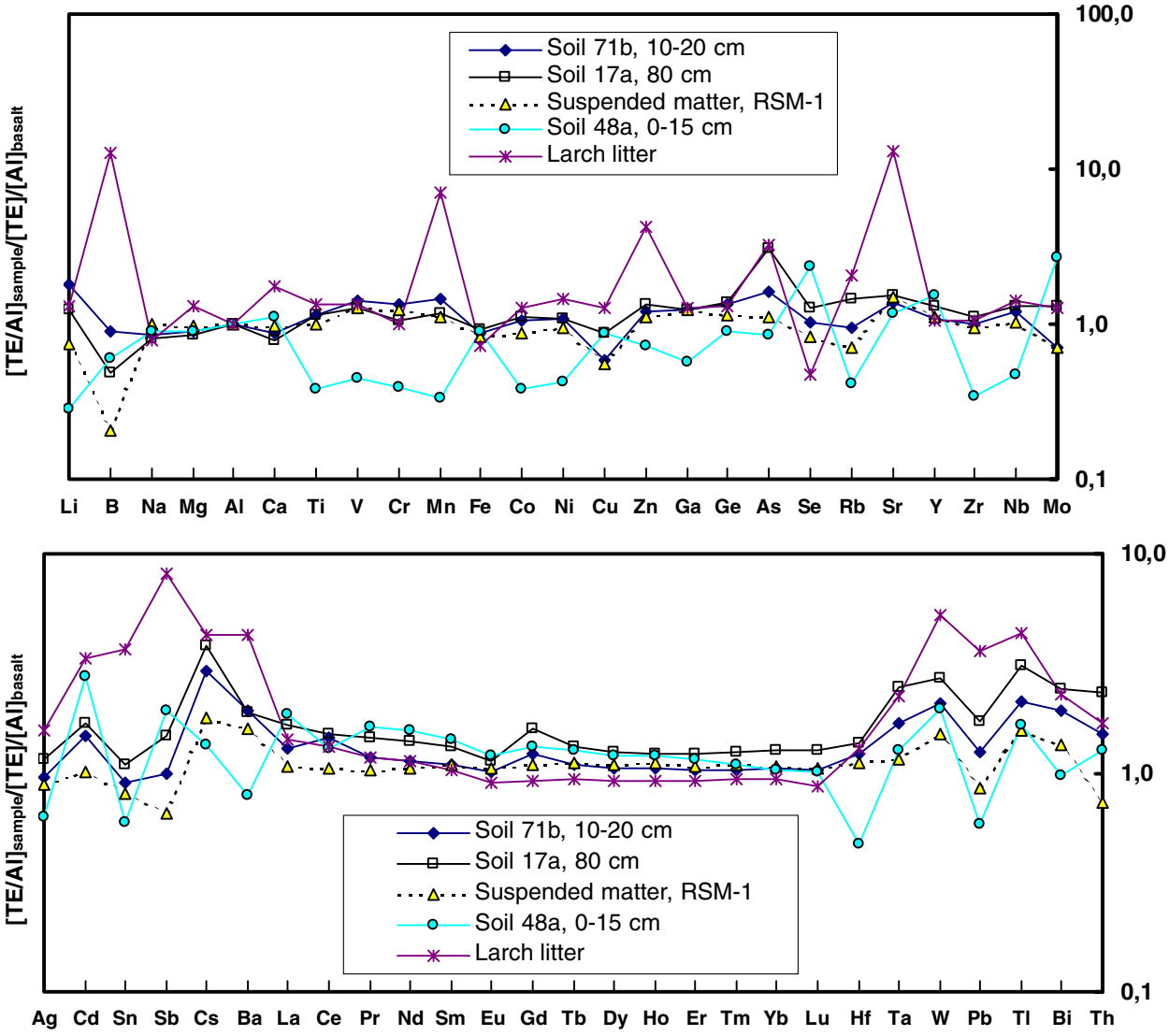

Fig. 9. Basalt-normalized TE concentrations in soil, plant litter and suspended matter.

3.3. Sources of TE and mechanisms of their migration

It is known that in boreal regions, rainwater percolation through the upper soil horizons down to the permafrost non-permeable level leads to enrichment in elements released during litter degradation and soil mineral dissolution (MacLean et al., 1999). This is supported by the observation that the major and trace element chemical composition of soil solutions is similar to that of neighboring rivers and groundwaters/suprapermafrost fluids (e.g., Nos. 54, 55; 3 and 4; 84–89). Analyses of porewaters from deep and surface soil horizons (i.e., 17a and 17b; 85a, 85b and 89) demonstrates only slight enrichments in the deep horizon and the absence of chemical transformation during lateral migration of soil porewaters (suprapermafrost flow) along the permafrost table to the river. Indeed, although the sample of surface soil solution (17b, 0–10 cm) exhibits concentrations that are a factor of 2 lower for most dissolved elements compared to the sample from the deep soil horizon (No. 17a, 80 cm), the iron-normalized ratio $([TE]/[Fe])_{deep}/([TE]/[Fe])_{surface}$ for most elements is equal to 1.0 ± 0.1, indicating the absence of chemical fractionation during downward migration of soil fluids.

Vegetation is known to be an important factor controlling the geochemistry of trace elements in continental environments representing a large pool of TE storage (Viers et al., 2005) and strongly contributing to TE cycling in cold, boreal climates (Dobrovolsky, 1988). We compared Al-normalized TE accumulation in litter to their concentrations in soil horizons and parent rocks (Fig. 9). These measurements reveal important enrichment of moss and lichens in Ti, V, Cr, Fe, Ga, Y, Zr, HREE (factor $\leqslant 2$), Li, Na, Mg, Ca, Ni, Cu, Ge, Y, Zr, Nb, LREE (factor 2–8), Mn, Zn, As, Se, Rb, Sr, Mo, Ag, Cd, Ba, Ta, W, Pb, Tl, Bi, Th, U (factor 10–100) and Sn(methyl?), Sb, Cs, Bi, Pb (factor > 100). This order is in fair agreement with trace element accumulation factors determined in Canadian lichens and mosses (Chiarenzelli et al., 2001).

Concentrations of trace metals in larch litter measured in the present study are close, within a factor of 2, to literature data for pine and spruce needles (Mn, Cu, Zn, Cd, Pb; Breymeyer et al., 1997; Ceburnis and Steinnes, 2000). The topsoil, containing 40-50% organic matter (No. 48a), is enriched in Se, Mo, Sn, Sb (Fig. 9), in accord with high concentration of these elements in the plant litter. Note that the relative enrichment of vascular plants leaves, compared to bedrock, in Zn, As, Se, Sr, Mo, Cd, Sb, Cs, Ba, Tl and Pb reported by Chiarenzelli et al. (2001) is consistent with results of the present study.

Considering the net primary production (NPP) of the region (90 g C/m^2 or ~180 t litter/km^2/y, Kajimoto et al., 1999) and taking into account TE content in larch litter (Table 4), one can calculate TE annual fluxes issued from the litter degradation. For this calculation, the ratio between the NPP and export flux of inorganic components from the upper soil horizon in the watershed (J) was taken as 0.8 which is consistent with results of long-term biogeochemical studies in the taiga zone (estimations of Bazilevich (1976) based on earlier works of Remezov et al. (1959) and Rodin and Bazilevich (1965)). These "litter-degradation" fluxes were found to be large enough to provide the full annual stream fluxes of many major (Si, Mg, Al, Fe) and all trace elements (Table 5). The importance of the biogenic pool of chemical elements has been recently recognized for other basaltic watersheds: analysis of Ge/Si ratio demonstrates that most of silica in water released to Hawaiian streams has passed through the biogenic silica pool, whereas direct mineral-water reactions account for only a small fraction of the stream silica flux (Derry et al., 2005).

Further insights on TE transport in the studied region can be gained by the analysis of REE behavior. The crust-normalized REE pattern of unaltered basalt (No. 55), various soil horizons (17a, 80 cm; 71b, 10–20 cm) and vegetation are relatively close to each other and distinctly different from that of soil porewaters, groundwaters and rivers (Fig. 10). All soil porewater fluids exhibit negative Ce anomaly and no positive Eu anomaly (except N 71b); no fractionation of REE is observed between the primary basalts, their alteration products (soils) and the vegetation. However, important fractionation consisting of appearance of Ce anomalies and slight enrichment in HREE takes place during REE mobilization from soil minerals or litter to soil porewaters and rivers. This fractionation can be explained by Ce oxidation and preferential HREE enrichment in solution during the REE coprecipitation/adsorption on Fe hydroxides or colloids from aqueous solution as supported by laboratory experiments (Bau, 1999). Note that the Ce anomaly is already pronounced in the topsoil horizon (0–15 cm) where the litter degradation occurs (sample 48a, Fig. 10A). The permafrost ice (No. 101, Fig. 10A) has a REE pattern that is broadly similar to the soil waters as it inherits the composition of summer solutions (Pokrovsky et al., 2005b).

Based on our results, the overall scheme of surface fluids enrichment in dissolved trace elements can be suggested

Table 4
Trace element composition of solid samples (in ppm)

	Green moss *Hylocomium s.*	Lichen *Cladonia s.*	Larch litter *Larix gmelinii*	RSM-1
Li	0.094	0.066	0.94	7.2
B	17.8	7.7	19.3	4.3
Na	234	118.0	906	15,880
Mg	934	161.0	3,440	35,040
Al	294	106	5,790	79,615
Ca	2,725	389	9,410	71,400
Ti	34.2	9.8	629	6497
V	1.0	0.2	19.9	265
Cr	0.8	0.2	10.0	167
Mn	384	80	563	1208
Fe	384	95	5100	78,330
Co	0.226	0.059	3.36	31.4
Ni	1.24	0.369	9.18	81.3
Cu	2.06	0.865	10.5	62.3
Zn	14.7	7.75	25.2	92.9
Ga	0.099	0.047	1.369	18.2
Ge	0.024	0.014	0.175	2.13
As	0.228	0.098	0.209	0.98
Se	0.124	0.209	0.155	3.72
Rb	5.46	1.90	2.34	11.0
Sr	21.2	2.35	128	200
Y	0.08	0.05	1.52	21.8
Zr	0.48	0.24	6.47	79.2
Nb	0.034	0.024	0.375	3.76
Mo	0.029	0.014	0.041	0.31
Ag	0.030	0.020	0.046	0.36
Cd	0.054	0.068	0.029	0.120
Sn	0.357	0.115	0.258	0.787
Sb	0.119	0.032	0.054	0.059
Cs	0.047	0.092	0.080	0.453
Ba	5.46	2.14	27.8	141
La	0.083	0.064	0.651	6.74
Ce	0.147	0.127	1.443	16.0
Pr	0.017	0.014	0.182	2.21
Nd	0.070	0.056	0.825	10.54
Sm	0.014	0.011	0.214	3.13
Eu	0.004	0.002	0.069	1.11
Gd	0.014	0.013	0.239	3.89
Tb	0.002	0.002	0.041	0.66
Dy	0.014	0.009	0.264	4.27
Ho	0.003	0.002	0.056	0.92
Er	0.009	0.005	0.163	2.60
Tm	0.001	0.001	0.023	0.37
Yb	0.009	0.004	0.151	2.35
Lu	0.001	0.001	0.022	0.36
Hf	0.011	ND	0.159	2.33
Ta	0.002	0.001	0.021	0.24
W	0.016	0.010	0.023	0.16
Pb	1.05	1.14	0.636	2.47
Tl	0.009	0.004	0.019	0.061
Bi	0.009	0.005	0.005	0.023
Th	0.015	0.014	0.133	1.07
U	0.020	0.007	0.050	0.302
	Soil SIB 48a	Soil SIB 71b	Soil 17a—80 cm	Basalt No. 55
Li	1.30	17.71	10.89	5.10
B	5.9	19.16	9.40	21.6
Na	6,680	13,653	11,722	16,320
Mg	15,400	32,220	28,080	37,200
Al	37,600	80,000	72,840	82,000
Ca	38,840	64,546	53,050	50,511
Ti	1,170	7,449	6,840	6,670
V	43.1	293	242	212

(*continued on next page*)

Table 4 (*continued*)

	Soil SIB 48a	Soil SIB 71b	Soil 17a—80 cm	Basalt No. 55
Cr	25.1	183.4	132.9	48.0
Mn	173	1,585	1,189	1,130
Fe	41,000	83,400	80,150	98,300
Co	6.57	38.0	36.6	37.2
Ni	17.0	92.9	85.1	88.3
Cu	47.3	66.7	91.7	117
Zn	28.1	99.6	100.2	84.9
Ga	4.01	18.7	16.9	15.3
Ge	0.788	2.50	2.33	1.901
As	0.355	1.44	2.53	0.914
Se	4.98	4.64	5.25	4.62
Rb	3.00	14.7	20.5	7.55
Sr	75.6	191	191.4	140
Y	14.1	21.2	23.3	20.3
Zr	13.6	83.3	85.3	86.2
Nb	0.809	4.46	4.418	3.77
Mo	0.569	0.314	0.528	0.456
Ag	0.122	0.390	0.428	0.420
Cd	0.154	0.175	0.184	0.123
Sn	0.274	0.891	0.974	1.005
Sb	0.082	0.091	0.123	0.093
Cs	0.161	0.752	0.896	0.263
Ba	32.9	173	152	91.7
La	5.56	8.24	9.53	6.55
Ce	9.33	22.0	21.07	15.65
Pr	1.64	2.50	2.83	2.19
Nd	7.4	11.4	12.8	10.4
Sm	1.91	3.16	3.45	2.96
Eu	0.60	1.08	1.11	1.09
Gd	2.23	4.42	5.20	3.70
Tb	0.356	0.654	0.721	0.614
Dy	2.24	4.16	4.49	4.04
Ho	0.472	0.87	0.935	0.859
Er	1.31	2.51	2.72	2.49
Tm	0.172	0.35	0.387	0.348
Yb	1.06	2.31	2.542	2.27
Lu	0.162	0.355	0.399	0.352
Hf	0.376	ND	0.687	2.33
Ta	0.049	0.271	0.274	0.226
W	0.083	0.232	0.307	0.141
Pb	1.53	3.44	4.09	1.71
Tl	0.02	0.09	0.115	0.075
Bi	0.011	0.031	0.041	0.008
Th	0.367	1.56	1.77	0.825
U	0.244	0.617	0.874	0.423

RSM = River Suspended Matter; ND = non-determined.

similar to that of the major dissolved components (Pokrovsky et al., 2005b). In summer, after the end of the snowmelt (July–beginning of September), percolating rainwater interacts with degrading plant litter/organic matter in the O(E) horizon and thus becomes enriched in OC and TE. From the end of the "active" period (second half of September–beginning of October), the freezing of these fluids in the confined space forms the ground ice that inherits the composition of soil fluids. During the following summer, the source of TE in surface waters reflects mixing of melting ground ice and infiltrating rainwater through the topsoil. Such a scenario is consistent with TE and OC mobilization from soil interstitial water and thawing ponds during melting of soil permafrost in spring and summer in Alaska (Rember and Trefry, 2004).

Table 5
Fluxes associated with plant litter degradation and their comparison with total dissolved fluxes

	Flux of litter degradation, g/km^2/y (J/NPP = 0.8)	Dissolved flux, g/km^2/y	Litter degradation, % of dissolved flux
Li	135	673	20
B	2,780	1,805	154
Mg	504,600	540,000	93
Na	130,000	2,220,000	6
Si	2,620,000	1,110,000	240
Al	834,000	11,300	7,400
Ca	1,360,000	3,000,000	45
Ti	90,530	1,190	7,600
V	2,860	388	737
Cr	1,440	125	1150
Mn	81,100	414	19,600
Fe	735,000	32,410	2,270
Co	483	16	3,000
Ni	1,322	264	501
Cu	1,520	1,040	146
Zn	3,630	519	700
As	30	35	86
Se	22	45	50
Rb	337	80	421
Sr	18,400	31,400	59
Y	219	113	194
Zr	931	230	405
Mo	6	8.61	69
Sn	37	4.5	825
Sb	8	4.1	188
Ba	4,000	123	3,250
La	94	25	375
Ce	208	39	533
Nd	119	43	276
Hf	23	5.1	448
Pb	92	4.5	2030
Th	19	2.7	710
U	7	3.3	219

4. Conclusions

The present study allows, for the first time, the quantitative assessment of TE concentrations and fluxes in pristine permafrost-dominated landscapes developed on trapps in Central Siberia. Similar to other boreal regions, colloidal transport of many insoluble trace elements (Fe, Al, Ti, Y, REE, Zr, Hf, Th) is the main feature revealed by ultrafiltration experiments. As a result of relatively humid climate and low runoff (for soluble elements) and both high concentration of dissolved organic matter and Fe–Al colloids (for insoluble elements), migration of most TE (Li, Sr, Sb, As, Mo, Se, Rb, Sn, Cu, Zn, Ni, Y, REEs, U, Zr, Hf, Th) occurs essentially in the dissolved (<0.22 μm), rather than in suspended form. In contrast to organic matter—dominated colloids of temperate and tropical zone, "boreal" colloids scavenge TE via coprecipitation and they are composed of Fe(Al)hydroxides stabilized by organic matter. Analyses of TE concentration in rocks, soils, suspended matter, plant litter and permafrost ice allowed for the characterization of possi-

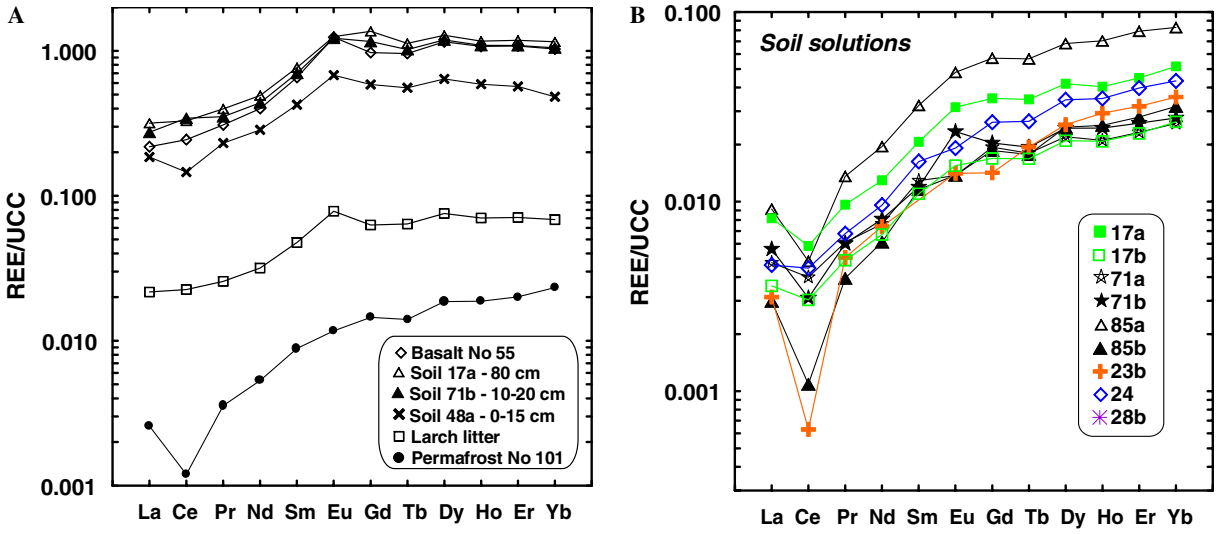

Fig. 10. Upper continental crust (UCC)-normalized REE pattern of rocks, soil and vegetation (A) and soil porewaters (B) in Central Siberia.

ble sources of elements in surficial fluids. We submit that the mobilization of TE from degrading plant litter in the surficial soil horizons is large enough to provide the annual dissolved fluxes of most of trace elements. A typical feature of basalt weathering in Central Siberia is the weak chemical element differentiation between source rocks, soil, river sediments and suspended matter. It is possible that, during the summer, rainwater interacts with degrading plant litter in the topsoil horizon leading to the formation of Fe–Al-organic colloids with incorporated TE. This is in contrast to permafrost-free environments, where TE–Fe colloids coprecipitation may occur during OM-stabilized iron oxy(hydr)oxides formation on the redox boundary of Fe(II)-rich waters with surficial DOC-rich horizons (Pokrovsky and Schott, 2002). The typical feature of Siberian landscapes developed on permafrost-dominated terrain is that migration of surficial fluids from the O(A) litter layer into deeper soil horizons and, along the permafrost table, to the rivers, occurs without important transformation of colloidal status and concentration ratios of TE.

Acknowledgements

This work was supported by the French program PNSE (Program National "Sol et Erosion") jointly funded by INSU/CNRS agencies. We thank Associate Editor Karen Johannesson, and two anonymous reviewers for their helpful comments that greatly improved the presentation and interpretation of results. Edward Sholkovitz is thanked for constructive review and fruitful discussion on ultrafiltration. The authors are grateful to F. Candaudap and C. Causserand for careful technical assistance during the analytical part of this study.

Associate editor: Karen Johannesson

Appendix A. Supplementary data

Supplementary data associated with this article can be found, in the online version, at doi:10.1016/j.gca.2006.04.008.

References

Allard, T., Menguy, N., Salomon, J., Calligaro, T., Weber, T., Calas, G., Benedetti, M.F., 2004. Revealing forms of iron in river-borne material from major tropical rivers of the Amazon Basin (Brazil). *Geochim. Cosmochim. Acta* **68**, 3079–3094.

Allison, J.D., Brown, D.S., Novo-Gradac, K.J., 1991. MINTEQA2/PRODEFA2, A geochemical assessment model for environmental systems: Version 3.0 user's manual. US EPA, Athens, GA.

Allison, J.D., Perdue, E.M., 1994. Modeling metal-humic interaction with Minteqa2. In: Senesi, N., Miano, T.M. (Eds.), *Humic Substances in the Global Environment and Implications on Human Health*. Elsevier Science B.V., Amsterdam, pp. 927–942.

Aries, S., Valladon, M., Polvé, M., Dupré, B., 2000. A routine method for oxide and hydroxide interference corrections in ICP-MS chemical analysis of environmental and geological samples. *Geostandard. Newslett.* **24**, 19–31.

Baes Jr., C.F., Mesmer, R.E., 1976. *The Hydrolysis of Cations*. John Wiley, New York.

Bau, M., 1999. Scavenging of dissolved yttrium and rare earths by precipitating iron oxyhydroxide: experimental evidence for Ce oxidation, Y-Ho fractionation, and lanthanide tetrad effect. *Geochim. Cosmochim. Acta* **63**, 67–77.

Bazilevich N.I., 1976. Biogenic and abiogenic processes in forest, step, and desert ecosystems. International Geography, 76, Section 4: Biogeography and Geography of Soils, pp. 58–62.

Benedetti, M.F., Milne, C.J., Kinnigurgh, D.G., Van Riemsdijk, W.H., Koopal, L.K., 1995. Metal ion binding to humic substances: Application of the non-ideal competitive adsorption model. *Environ. Sci. Technol.* **29**, 446–457.

Benoit, G., 1995. Evidence of the particle concentration effect for lead and other metals in freshwaters based on ultraclean technique analysis. *Geochim. Cosmochim. Acta* **59**, 2677–2687.

Botch, M.S., Kobak, K.I., Vinson, T.S., Kolchugina, T.P., 1995. Carbon pools and accumulation in peatlands of the former Soviet Union. *Global Biogeochem. Cycles* **9**, 37–46.

Braun, J.-J., Viers, J., Dupré, B., Polvé, M., Ndam, J., Muller, J.-P., 1998. Solid/liquid REE fractionation in the lateritic system of Goyoum, East Cameroon: the implication for the present dynamics of the soil covers of the humid tropical regions. *Geochim. Cosmochim. Acta* **62**, 273–299.

Breymeyer, A., Degorski, M., Reed, D., 1997. Decomposition of pine-litter organic matter and chemical properties of upper soil layers: transect studies. *Environ. Pollut.* **98**, 361–367.

Brown, J., Grant, C.L., Ugolini, F.C., Tedrow, J.C.F., 1962. Mineral composition of some drainage waters from arctic Alaska. *J. Geophys. Res.* **67**, 2447–2453.

Buffle, J., Perret, D., Newman, M., 1992. The use of filtration and ultrafiltration for size fractionation of aquatic particles, colloids and macromolecules. In: Buffle, J., van Leeuwen, H.P. (Eds.), *Environmental Particles*, vol. 1. Lewis Publishers, Boca Raton, FL, pp. 171–230, Chapter 5.

Ceburnis, D., Steinnes, E., 2000. Conifer needles as biomonitors of atmospheric heavy metal deposition: comparison with mosses and precipitation, role of the canopy. *Atmos. Environ.* **34**, 4265–4271.

Chesworth, W., Dejou, J., Larroque, P., 1981. The weathering of basalt and relative mobilities of the major elements at Belbex, France. *Geochim. Cosmochim. Acta* **45**, 1235–1243.

Chiarenzelli, J., Aspler, L., Dunn, C., cousens, B., Ozarko, D., Powis, K., 2001. Multi-element and rare earth element composition of lichens, mosses, and vascular plants from the Central Barrenlands, Nunavut, Canada. *Appl. Geochem.* **16**, 245–270.

Dai, M.-H., Martin, J.-M., 1995. First data on trace metal level and behaviour in two major Arctic river-estuarine systems (Ob and Yenisey) and in the adjacent Kara Sea, Russia. *Earth Planet. Sci. Lett.* **131**, 127–141.

Derry, L.A., Kurtz, A.C., Ziegler, K., Chadwick, O.A., 2005. Biological control of terrestrial silica cycling and export fluxes to watersheds. *Nature* **433**, 728–731.

Dia, A., Gruau, G., Olivié-Lauquet, G., Riou, C., Molénat, J., Curmi, P., 2000. The distribution of rare earth elements in groundwaters: assessing the role of source-rock composition, redox changes and colloidal particles. *Geochim. Cosmochim. Acta* **64**, 4131–4151.

Dobrovolsky, V.V., 1988. Heavy-metal biogeochemical cycles. *Geochem. Internat.* (No. 2), 137–147.

Dupré, B., Gaillardet, J., Rousseau, D., Allègre, C.J., 1996. Major and trace element of river-born material: the Congo Basin. *Geochim. Cosmochim. Acta* **60**, 1301–1321.

Dupré, B., Viers, J., Dandurand, J.-L., Polve, M., Bénézeth, P., Vervier, Ph., Braun, J.-J., 1999. Major and trace elements associated with colloids in organic-rich river waters: ultrafiltration of natural and spiked solutions. *Chem. Geol.* **160**, 63–80.

Dupré, B., Dessert, C., Oliva, P., Goddéris, Y., Viers, J., Francois, L., Millot, R., Gaillardet, J., 2003. Rivers, chemical weathering and Earth's climate. *C.R. Geoscience* **335**, 1141–1160.

Dzombak, D.A., Morel, F.M.M., 1990. *Surface Complexation Modeling—Hydrous Ferric Oxide*. Wiley, New York.

Erel, Y., Morgan, J.J., Patterson, C.C., 1991. Natural levels of lead and cadmium in a remote mountain stream. *Geochim. Cosmochim. Acta* **55**, 707–719.

Everett, K.R., Kane, D.L., Hinzman, D.L., 1996. Surface water chemistry and hydrology of a small arctic drainage basin. In: Reynolds, J.F., Tenhunen, J.D. (Eds.), *Landscape Function and Disturbance in Arctic Tundra*, *Ecological Studies*, 120. Springer, Berlin, pp. 185–201.

Eyrolle, F., Benaim, J.-Y., 1999. Metal available sites on colloidal organic compounds in surface waters (Brazil). *Water Res.* **33**, 995–1004.

Gaillardet J., Viers J., Dupre B., 2003. Trace elements in river waters, In: Drever, J.I. (Ed.), *Surface and Ground Water, Weathering, Erosion and Soils*. In: Holland, H.D., Turekian K.K. (Eds.), *Treatise of Geochemistry*, vol. 5, Elsevier-Pergamon, Oxford. pp. 225–272.

Gordeev, V.V., Martin, J.-M., Sidorov, I.S., Sidorova, M.V., 1996. A reassessment of the Eurasian river input of water, sediment, major elements, and nutrients to the Arctic Ocean. *Am. J. Sci.* **296**, 664–691.

Gordeev, V.V., Rachold, V., Vlasova, I.E., 2004. Geochemical behaviour of major and trace elements in suspended particulate material of the Irtysh river, the main tributary of the Ob river, Siberia. *Appl. Geochem.* **19**, 593–610.

Guieu, C., Huang, W.W., Martin, J.-M., Yong, Y.Y., 1996. Outflow of trace metals into the Laptev Sea by the Lena River. *Marine Chem.* **53**, 255–267.

Guo, L., Santschi, P.H., 1996. A critical evaluation of the cross-flow ultrafiltration technique for the sampling of colloidal organic in seawater. *Marine Chem.* **55**, 113–128.

Guo, L., Semiletov, I., Gustafsson, O., Ingri, J., Andersson, P., Dudarev, O., White, D., 2004. Characterization of Siberian Arctic coastal sediments: implications for terrestrial organic carbon export. *Global Biogeochem. Cycles* **18**, GB 1036. doi:10.1029/2003GB002087.

Hoffman, M.R., Yost, E.C., Eisenreich, S.J., Maier, W.L., 1981. Characterization of soluble and colloidal-phase complexes in river water by ultrafiltration. A mass balance approach. *Environ. Sci. Technol.* **15**, 655–661.

Hoffmann, S.R., Shafer, M.M., Babiarz, C.L., Armstrong, D.E., 2000. A critical evaluation of tangential-flow ultrafiltration for trace metal studies in freshwater systems. 1. Organic carbon. *Environ. Sci. Technol.* **34**, 3420–3427.

Ingri, J., Widerlund, A., Land, M., Gustafsson, O., Andersson, P., Ohlander, B., 2000. Temporal variations in the fractionation of the rare earth elements in a boreal river; the role of colloidal particles. *Chem. Geol.* **166**, 23–45.

Ingri, J., Nordling, S., Larsson, J., Ronnegard, J., Nilsson, N., Rodushkin, I., Dahlqvist, R., Andersson, P., Gustafsson, O., 2004. Size distribution of colloidal trace metal and organic carbon during a coastal bloom in the Baltic Sea. *Marine Chem.* **91**, 117–130.

Johannesson, K.H., Lyons, W.B., Graham, E.Y., Welch, K.A., 2000. Oxyanion concentrations in Eastern Sierra Nevada Rivers—3. Boron, molybdenum, vanadium, and tungsten. *Aquat. Geochem.* **6**, 19–46.

Johannesson, K.H., Tang, J., Daniels, J.M., Bounds, W.J., Burdige, D.J., 2004. Rare earth element concentrations and speciation in organic-rich blackwaters of the Great Dismal Swamp, Virginia, USA. *Chem. Geol.* **209**, 271–294.

Kajimoto, T., Matsura, Y., Sofronov, M.A., Volokitina, A.V., Mori, S., Osawa, A., Abaimov, A.P., 1999. Above- and belowground biomass and net primary productivity of a *Larix gmelinii* stand near Tura, central Siberia. *Tree Physiol.* **19**, 815–822.

Kononova, M.M., 1963. Organic matter of soils. Its nature, properties and investigation methods. *Moscow, Izd-vo Acad. Sci. USSR* (in Russian).

Konhauser, K.O., Fyfe, W.S., Kronberg, B.I., 1994. Multi-element chemistry of some Amazonian waters and soils. *Chem. Geol.* **111**, 155–175.

Lahermo, P., Mannio, J., Tarvainen, T., 1995. The hydrogeochemical comparison of streams and lakes in Finland. *Appl. Geochem.* **10**, 45–64.

Lead, J.R., Davison, W., Hamilton-Taylor, J., Buffle, J., 1997. Characterizing colloidal material in natural waters. *Aquat. Geochem.* **3**, 213–232.

Lock, M.A., Ford, T.E., 1986. Colloidal and dissolved organic carbon dynamics in undisturbed boreal forest catchments: A seasonal study of apparent molecular weight spectra. *Freshwater Biol.* **16**, 187–195.

Lock, M.A., Ford, T.E., Fiebig, D.M., Miller, M.C., Hullar, M., Kaufman, M., Vetsall, J.R., Peterson, B.J., Hobbie, J.E., 1989. A biogeochemical survey of rivers and streams in the mountains and foothills province of arctic Alaska. *Arch. Hydrobiol.* **115**, 499–521.

Louvat, P., Allégre, C.J., 1997. Present denudation rates on the island of Reunion determined by river geochemistry: basalt weathering and mass budget between chemical and mechanical erosions. *Geochim. Cosmochim. Acta* **61**, 3645–3669.

Louvat, P., Allégre, J.C., 1998. Riverine erosion rates on Sao Miguel volcanic island, Azores archipelago. *Chem. Geol.* **148**, 177–200.

Lyvén, B., Hassellov, M., Turner, D.R., Haraldsson, C., Andersson, K., 2003. Competition between iron- and carbon-based colloidal carriers for trace metals in a freshwater assessed using a flow field-flow fractionation coupled to ICPMS. *Geochim. Cosmochim. Acta* **67**, 3791–3802.

MacLean, R., Oswood, M.W., Irons III, J.G., McDowell, W.H., 1999. The effect of permafrost on stream biogeochemistry: a case study of two streams in the Alaskan (USA) taiga. *Biogeochemistry* **47**, 239–267.

Martell, A.E., Smith, R.M., Motekaitis, R.J., 1997. NIST Critically selected stability constants of metal complexes. Database software Version 3.0. Texas A&M University, College Station, TX.

Martin, J.M., Guan, D.M., Elbaz-Poulichet, F., Thomas, A.J., Gordeev, V.V., 1993. Preliminary assessment of the distribution of some trace elements (As, Cd, Cu, Fe, Ni, Pb and Zn) in a pristine aquatic environment: the Lena River estuary (Russia). *Marine Chem.* **43**, 185–199.

Millot, R., Gaillardet, J., Dupré, B., Allègre, C.J., 2003. Northern latitude chemical weathering rates: Clues from the Mackenzie River Basin, Canada. *Geochim. Cosmochim. Acta* **67**, 1305–1329.

Moran, S.B., Woods, W.L., 1997. Cd, Cr, Cu, Ni and Pb in the water column and sediments of the Ob-Irtysh Rivers, Russia. *Mar. Poll. Bull.* **35**, 270–279.

Morrison, M.A., Benoit, G., 2001. Filtration artifacts caused by overloading membrane filters. *Environ. Sci. Technol.* **35**, 3774–3779.

Oliver, B.G., Thurman, E.M., Malcolm, R.L., 1983. The contribution of humic substances to the acidity of colored natural waters. *Geochim. Cosmochim. Acta* **47**, 2031–2035.

Olivié-Lauquet, G., Allard, Th., Benedetti, M., Muller, J.-P., 1999. Chemical distribution of trivalent iron in riverine material from a tropical ecosystem: a quantitative EPR study. *Water Res.* **33**, 2726–2734.

Olivié-Lauquet, G., Allard, Th., Bertaux, J., Muller, J.-P., 2000. Crystal chemistry of suspended matter in a tropical hydrosystem, Nyong basin (Cameroon, Africa). *Chem. Geol.* **170**, 113–131.

Oswood, M.W., Irons III, J.G., Schell, D.M., 1996. Dynamics of dissolved and particulate carbon in a tundra stream in arctic Alaska. In: Reynolds, J.F., Tenhunen, J.D. (Eds.), *Landscape Function and Disturbance in Arctic Tundra*, *Ecological Studies*, 120. Springer, Berlin, pp. 275–287.

Palmer, M.R., Edmond, J.M., 1993. Uranium in river water. *Geochim. Cosmochim. Acta* **57**, 4947–4955.

Peng, C., Apps, M.J., Price, D.T., Nalder, I.A., Halliwell, D.H., 1998. Simulating carbon dynamics along the Boreal Forest Transect Case Study (DFTCS) in Central canada, 1, Model testing. *Global Biogeochem. Cycles* **12**, 381–392.

Peterson, B.J., Hobbie, J.E., Corliss, T.L., 1986. Carbon flow in a tundra stream ecosystem. *Can. J. Fish. Aquat. Sci.* **43**, 1259–1270.

Peterson, B.J., Corliss, T., Kriet, K., Hobbie, J.E., 1992. Nitrogen and phosphorus concentrations and export for the upper Kuparak River on the North Slope of Alaska in 1980. *Hydrobiology* **240**, 61–69.

Pokrovsky, O.S., Schott, J., 2002. Iron colloids/organic matter associated transport of major and trace elements in small boreal rivers and their estuaries (NW Russia). *Chem. Geol.* **190**, 141–179.

Pokrovsky, O.S., Dupré, B., Schott, J., 2005a. Fe–Al-organic colloids control of trace elements in peat soil porewaters: results of ultrafiltration and dialysis. *Aquat. Geochem.* **11**, 241–278.

Pokrovsky, O.S., Schott, J., Kudryavtzev, D.I., Dupré, B., 2005b. Basalts weathering in Central Siberia under permafrost conditions. *Geochim. Cosmochim. Acta* **69**, 5659–5680.

Pokrovsky O.S., Pokrovski G.S., Schott J., Galy A., 2006. Experimental study of germanium adsorption on goethite and Ge coprecipitation with iron hydroxide: X-ray absorption fine structure and macroscopic characterization. *Geochim. Cosmochim. Acta*, in press, doi:10.1016/j.gca.2006.04.012.

Polynov, B.B., 1944. Modern objects of weathering study (Sovremennye zadachi ucheniya o vyvetrivanii). *Izv. Acad. Nauk SSSR, Ser. Geol.* (No. 2), 3–14.

Porcelli, D., Andersson, P.S., Wasserburg, G.J., Ingri, J., Baskaran, M., 1997. The importance of colloids and mires for the transport of uranium isotopes through the Kalix River watershed and Baltic Sea. *Geochim. Cosmochim. Acta* **61**, 4095–4113.

Prokushkin, A.S., Kajimoto, T., Prokushkin, S.G., McDowell, W.H., Abaimov, A.P., Matsuura, Y., 2005. Climatic factors influencing fluxes of dissolved organic carbon from the forest floor in a continuous-permafrost Siberian watershed. *Can. J. Forest Res.* **35**, 2130–2140.

Rember, R.D., Trefry, J.H., 2004. Increased concentrations of dissolved trace metals and organic carbon during snowmelt in rivers of the Alaskan Arctic. *Geochim. Cosmochim. Acta* **68**, 477–489.

Remezov, N.P., Bykova, L.N., Smirnova, K.M., 1959. *Utilization and Turnover of Nitrogen and Ash Elements in Forests of the European Part of the USSR*. Publ. House of Moscow State University, 284 pp. (in Russian).

Rode, A.A., 1937. Podzol-forming process (Podzoloobrazovatelnyi protzess). *Moscow-Leningrad, Izd-vo Acad. Sci. USSR* (in Russian).

Rodin, L.E., Bazilevich, N.I., 1965. *Dynamics of the Organic Matter and Biological Turnover of Ash Elements and Nitrogen in the Main Types of the World Vegetation*. Nauka Publ. House, Moscow-Leningrad, 251 pp. (in Russian).

Rose, J., Vilge, A., Olivie-Lauquet, G., Masion, A., Frechou, C., Bottero, J.-Y., 1998. Iron speciation in natural organic matter colloids. *Colloid. Surfaces A* **136**, 11–19.

Ross, J.M., Sherrell, R.M., 1999. The role of colloids in trace metal transport and adsorption behavior in New Jersey Pinelands streams. *Limnol. Oceanogr.* **44**, 1019–1034.

Schafer, Th., Artinger, R., Dardenne, K., Bauer, A., Schuessler, W., Kim, J.I., 2003a. Colloid-borne americum migration in Gorleben groundwater: significance of iron secondary phase transformation. *Environ. Sci. Technol.* **37**, 1528–1534.

Schafer, Th., Hertkorn, N., Artinger, R., Claret, F., Bauer, A., 2003b. Functional group analysis of natural organic colloids and clay association kinetics using C(1s) spectromicroscopy. *J. Phys. IV (France)* **104**, 409–412.

Serreze, M.C., Bromwich, D.H., Clark, M.P., Etringer, A.J., Zhang, T.J., Lammers, R., 2002. Large-scale hydro-climatology of the terrestrial Arctic drainage system. *J. Geophys. Res.-Atmos.* **108** (D2). Art. No. 8160.

Shiller, A.M., 2003. Syringe filtration methods for examining dissolved and colloidal trace element distributions in remote field locations. *Environ. Sci. Technol.* **37**, 3953–3957.

Sholkovitz, E.R., 1992. Chemical evalution of rare-earth elements: fractionation between colloidal and solution phases of filtered river water. *Earth Planet. Sci. Lett.* **114**, 77–84.

Sholkovitz, E.R., 1995. The aquatic chemistry of rare earth elements in rivers and estuaries. *Aquat. Geochem.* **1**, 1–34.

Sigg, L., Xue, H., Kistler, D., Schönenberger, R., 2000. Size fractionation (dissolved, colloidal and particulate) of trace metals in Thur River, Switzerland. *Aquat. Geochem.* **6**, 413–434.

Sonke, J.E., Salters, V.J.M., 2006. Lanthanide–humic substances complexation. I. Experimental evidence for a lanthanide contraction effect. *Geochim. Cosmochim. Acta* **70**, 1495–1506.

Tang, J., Johannesson, K.H., 2003. Speciation of rare earth elements in natural terrestrial waters: Assessing the role of dissolved organic matter from the modeling approach. *Geochim. Cosmochim. Acta* **67**, 2321–2339.

Targulian V.O., 1971. Soil formation and weathering in cold humid regions (on massive-crystalline and sandy polymictic rocks). Moscow, Nauka. (in Russian).

Tipping, E., 1994. WHAM: a chemical equilibrium model and computer code for waters, sediments and soils incorporating a discrete site/electrostatic model of ion-binding by humic substances. *Comput. Geosci.* **20**, 973–1023.

Trumbore, S.E., Harden, J.W., 1997. Accumulation and turnover of carbon in organic and mineral soils of the BOREAS northern study area. *J. Geophys. Res.* **102** (D24), 28817–28830.

Ugolini, F.C., Stoner, M.G., Marrett, D.J., 1987. Arctic pedogenesis: 1. Evidence for contemporary podzolization. *Soil. Sci.* **144**, 90–100.

Viers, J., Dupré, B., Polvé, M., Schott, J., Dandurand, J.-L., Braun, J.-J., 1997. Chemical weathering in the drainage basin of a tropical watershed (Nsimi-Zoetele site, Cameroon): comparison between organic-poor and organic-rich waters. *Chem. Geol.* **140**, 181–206.

Viers, J., Barroux, G., Pinelli, M., Seyler, P., Oliva, P., Dupré, B., Boaventura, G.R., 2005. The influence of the Amazonian floodplain ecosystems on the trace element dynamics of the Amazon River mainstream (Brazi). *Sci. Total Environ.* **339**, 219–232.

Wilkinson, K.J., Nègre, J.-C., Buffle, J., 1997. Coagulation of colloidal material in surface waters: the role of natural organic matter. *J. Contamin. Hydrology* **26**, 229–243.

Yeghicheyan, D., Carignan, J., Valladon, M., Le Coz, M.B., Aquilina, L., et al., 2001. A compilation of some trace elements measured in the natural river water standard SLRS-4 (NRC-CNRS). *Geostandard. Newslett.* **25**, 468–474.

Zhulidov, A.V., Headey, J.V., Robarts, R.D., Nikanorov, A.M., Ishenko, A.A., Champ, M.A., 1997. Concentrations of Cd, Pb, Zn and Cu in pristine wetlands of the Russian Arctic. *Mar. Poll. Bull.* **35**, 242–251.

Zolotukhin, V.V., Al'Mukhamedov, A.I., 1988. Traps of the Siberian Platfrom. In: Macdougall, J.D. (Ed.), *Continental Flood Basalts*. Kluwer Academic Publishers, Dordrecht, pp. 273–310.